

Neutrino Mass Textures and Partial $\mu - \tau$ Symmetry

E. I. Lashin^{1,2,3*}, N. Chamoun^{4,5†}, C. Hamzaoui^{6‡}, and S. Nasri^{7,8§}

¹ Ain Shams University, Faculty of Science, Cairo 11566, Egypt.

² Centre for Theoretical Physics, Zewail City of Science and Technology,
Sheikh Zayed, 6 October City, 12588, Giza, Egypt.

³ The Abdus Salam ICTP, P.O. Box 586, 34100 Trieste, Italy.

⁴ Physics Department, HIAST, P.O.Box 31983, Damascus, Syria.

⁵ Physikalisches Institut der Universität Bonn, Nußalle 12, D-53115 Bonn, Germany.

⁶ Groupe de Physique Théorique des Particules,
Département des Sciences de la Terre et de L'Atmosphère,
Université du Québec à Montréal, Case Postale 8888, Succ. Centre-Ville,
Montréal, Québec, Canada, H3C 3P8.

⁷ Department of Physics, UAE University, P.O.Box 17551, Al-Ain, United Arab Emirates.

⁸ Laboratoire de Physique Théorique, ES-SENIA University, DZ-31000 Oran, Algeria.

March 1, 2022

Abstract

We discuss the viability of the $\mu - \tau$ interchange symmetry imposed on the neutrino mass matrix in the flavor space. Whereas the exact symmetry is shown to lead to textures of completely degenerate spectrum which is incompatible with the neutrino oscillation data, introducing small perturbations into the preceding textures, inserted in a minimal way, lead however to four deformed textures representing an approximate $\mu - \tau$ symmetry. We motivate the form of these ‘minimal’ textures, which disentangle the effects of the perturbations, and present some concrete realizations assuming exact $\mu - \tau$ at the Lagrangian level but at the expense of adding new symmetries and matter fields. We find that all these deformed textures are capable to accommodate the experimental data, and in all types of neutrino mass hierarchies, in particular the non-vanishing value for the smallest mixing angle.

Keywords: Neutrino masses, **PACS numbers:** 14.60.Pq; 11.30.Hv; 14.60.St

1 Introduction

The elusive neutrino particles proved, so far, to be the only feasible window for the physics beyond the Standard Model (SM) of particle physics. The observed solar and atmospheric neutrino oscillations in the Super-Kamiokande [1] experiment constitute a compelling evidence for the massive nature of neutrinos which is a clear departure from the SM particle physics. In the flavor basis where the charged lepton mass matrix is diagonal, the mixing can be solely attributed to the effective neutrino mass matrix M_ν . In such

*slashin@zewailcity.edu.eg, elashin@ictp.it

†nchamoun@th.physik.uni-bonn.de

‡hamzaoui.cherif@uqam.ca

§snasri@uaeu.ac.ae

a case the neutrino mass matrix M_ν can be parameterized by nine free parameters: three masses (m_1 , m_2 and m_3), three mixing angles (θ_x , θ_y and θ_z) and three phases (two Majorana-type ρ , σ and one Dirac-type δ). The culmination of experimental data [2, 3, 4, 5] amounts to constraining the masses and the mixing angles, while for the phases there is no, so far, a feasible experimental set for their determination. The recent results from the T2K[6], MINOS[7], and Double Chooz[8] experiments reveal a nonzero value of θ_z . The more recent Daya Bay [9] and RENO[10] experiments confirm a sizable value with relatively high precision. The discovery of relatively large mixing angle θ_z has a tremendous impact on searching for a sizable CP-violation effect in neutrino oscillations that enables measuring the Dirac phase δ . The impact could also extend to our understanding of matter-antimatter asymmetry that shaped our universe.

In order to cope with a relatively large mixing angle θ_z , one might be compelled to introduce new ideas in model building that may enrich our theoretical understanding of the neutrino flavor problem or the flavor problem in general in case we are fortunate enough. One of the common ideas, often discussed in the literature[11], is using flavor symmetries, and one of the most attractive ideas in this regard is the μ - τ symmetry [12, 13]. This symmetry is enjoyed by many popular mixing patterns such as tri-bimaximal mixing (TBM) [14], bimaximal mixing (BM) [15], hexagonal mixing (HM) [16] and scenarios of A_5 mixing [17], and it was largely studied in the literature [18]. Actually, many sorts of these symmetries happen to be ‘accidental’ - just a numerical coincidence of parameters without underlying symmetry, but rather a symmetry resulting from a mutual influence of different and independent factors. The authors of [19] showed that the TBM symmetry falls under this category in that large deviations from its predictions are allowed experimentally. Nonetheless, one can adopt a more ‘fundamental’ approach and construct models incorporating the symmetry in question at the Lagrangian level. In this context, recent, particularly simple, choices for discrete and continuous flavor symmetry addressing the non-vanishing θ_z question were respectively worked out in [20] and [21].

For the μ - τ symmetry, it is well known that the exact form often requires vanishing θ_z and, thus, the recent results on non-vanishing θ_z force us to abandon the idea of exact μ - τ symmetry and to invoke small perturbation violating it. The idea of introducing perturbations over a μ - τ symmetric mass matrix was recently introduced in [22, 23, 24], where the authors analyzed the effect of perturbations and the correlation of their sizes with those corresponding to the deviation of θ_z and $\theta_y - \frac{\pi}{4}$ from zero. In [22], the perturbations are introduced into the μ - τ symmetric neutrino mass matrix at all entries, while in [23] the perturbations are introduced only at the mass matrix entries which are related through μ - τ symmetry. The perturbations in [24] were imposed on four and three zero neutrino Yukawa textures. In fact, approximate interchange symmetry between second and third generation fields goes back to [25] where μ - τ symmetry was extended to all fermions with a concrete realization in a two-doublets Higgs model.

In this present work, we follow a similar procedure as in [23], and insert the perturbations only at mass matrix entries related by μ - τ symmetry. In our approach, however, the deformed relations are thought of as defining textures, and this way of thinking provides deep insight about the μ - τ symmetry itself and its breaking. The two relations defining the approximately μ - τ symmetric texture contain two parameters, generally complex, controlling the strength of the symmetry breaking. For the sake of simplicity and clarity, we disentangle each parameter to be kept alone in the relations defining the texture. The ‘minimal’ textures obtained in this way (minimal in the sense of containing just one symmetry breaking parameter) may be considered as a ‘basis’ for all perturbations. Moreover, the numerical study of [23] with normal hierarchy spectrum required one of the two symmetry breaking parameters to be small with respect to the other, and this motivated us to consider the extreme case where one of the two symmetry breaking parameters is absent.

As we shall see, the exact μ - τ symmetry can be realized in two different ways as equating to zero two linear combinations of the mass matrix entries. Thus, upon deforming these two defining linear combinations, in each of the possible two ways of realizing μ - τ symmetry, by two parameters (each parameter affecting one linear combination) and separating the two parameters effects, we end up with four possible textures. The two equations defining each textures provide us with four real equations, which are used to reduce the independent parameters of the neutrino mass matrix in this specific texture from nine to five. We choose the five input parameters to be the mixing angles ($\theta_x, \theta_y, \theta_z$), the Dirac phase δ and the solar mass square difference δm^2 , and we vary them within their experimentally acceptable

regions. Moreover, we vary also the complex parameter defining the deformation. Therefore, in this way we can reconstruct the neutrino mass matrix out of 7-dimensional parameter space, and compute the unknown mass spectrum (m_1, m_2, m_3) and the two Majorana phases ρ and σ . We perform consistency check with the other experimental results, and find that all possible four textures could accommodate the data. However, no singular models, where one of the masses equals zero, could be viable.

In contrast to the analysis of [23] which stated that normal type hierarchy is not compatible with small perturbations ($\epsilon < 20\%$), we found all the patterns viable in all types of mass hierarchies (normal, inverted and quasi-degenerate) for even smaller perturbations ($\chi = 2\epsilon < 20\%$). The different conclusions are due to two factors. First, in [23] the phase angles are varied whereas the mixing angles and the other observables are fixed to their central values, which corresponds to narrow slices in the parameter space we adopted in our work. Second, the definition of normal hierarchy in our work ($m_1/m_3 < m_2/m_3 < 0.7$) is less restricted than the definition adopted in [23] ($m_1 \ll m_2 \ll m_3$). Thus we believe our analysis is more thorough and our conclusions are more solid.

As to the origin of the perturbations, there are few strategies to follow. First, one can add terms violating explicitly the $\mu - \tau$ symmetry in the Lagrangian, as was done in [26]. Second, one may assume exact symmetry, leading to $\theta_z = 0$, at high scale. Then renormalization group (RG) running of the neutrino mass matrix elements creates a term which breaks the $\mu - \tau$ symmetry at the electroweak scale. However, many studies showed that the RG effects are negligible. In [27], this process of symmetry breaking via RG running within multiple Higgs doublets model was only valid, for a sizable θ_z , in a quasi-degenerate spectrum. In [28], the same conclusion, about the inability of radiative breaking to generate relatively large θ_z , was reached in minimal supersymmetric standard model (MSSM) schemes. Thus, we shall not consider RG effects, but impose approximate $\mu - \tau$ symmetry at high scale (seesaw scale, say) which would remain valid at measurable electroweak scale. Third, as was done in [29], the $\mu - \tau$ symmetry is replaced by another symmetry including the former as a subgroup. In this spirit and in line with [23, 25], we address in detail the question of the perturbations root and present some concrete examples at the Lagrangian level for the ‘minimal’ texture form having only one breaking parameter by means of adding extra Higgs fields and symmetries, in both types I and II of seesaw mechanisms. In type II seesaw, we achieve the desired perturbed form by adding a new Z_2 -symmetry to the one characterizing the $\mu - \tau$ symmetry (which we denote henceforth by S) and three Higgs triplets responsible for giving masses to the left-handed (LH) neutrinos and by substituting three Higgs doublets for the SM Higgs field for the charged lepton masses. On the other hand, we achieve the desired form in type I seesaw by considering a flavor symmetry of the form $S \times Z_8$ and by having three SM-like Higgs doublets for the charged leptons masses, four other Higgs doublets for the Dirac neutrino mass matrix and additional two Higgs singlets for the Majorana right-handed (RH) neutrino mass matrix.

The plan of the paper is as follows: in section 2, we review the standard notation for the neutrino mass matrix and its relation to the experimental constraints. In section 3, we present the $\mu - \tau$ symmetry and its implications. The realization of $\mu - \tau$ symmetry as textures and its consequences for non-singular and singular cases are respectively worked out in section 4 and 5. In section 6, we present the minimal possible ways for breaking the $\mu - \tau$ symmetry leading to four cases being interpreted as four possible textures, and we classify all the hierarchy patterns regarding the mass spectra. The detailed relevant formulae and the results of the phenomenological analysis of each texture are presented in Section 7 (for nonsingular cases) and Section 8 (for singular ones). In section 9, we present a possible Lagrangian for the approximate $\mu - \tau$ leading to the ‘minimal’ textures we adopted. The last section 10 is devoted for discussions and conclusions.

2 Standard notation

In the flavor basis, where the charged lepton mass matrix is diagonal, we diagonalize the symmetric neutrino mass matrix M_ν by a unitary transformation,

$$V^\dagger M_\nu V^* = \begin{pmatrix} m_1 & 0 & 0 \\ 0 & m_2 & 0 \\ 0 & 0 & m_3 \end{pmatrix}, \quad (1)$$

with m_i (for $i = 1, 2, 3$) real and positive. We introduce the mixing angles $(\theta_x, \theta_y, \theta_z)$ and the phases (δ, ρ, σ) such that [30]:

$$\begin{aligned} V &= UP \\ P &= \text{diag}(e^{i\rho}, e^{i\sigma}, 1) \\ U &= \begin{pmatrix} c_x c_z & s_x c_z & s_z \\ -c_x s_y s_z - s_x c_y e^{-i\delta} & -s_x s_y s_z + c_x c_y e^{-i\delta} & s_y c_z \\ -c_x c_y s_z + s_x s_y e^{-i\delta} & -s_x c_y s_z - c_x s_y e^{-i\delta} & c_y c_z \end{pmatrix}, \end{aligned} \quad (2)$$

(with $s_x \equiv \sin \theta_x \dots$) to have

$$M_\nu = U \begin{pmatrix} \lambda_1 & 0 & 0 \\ 0 & \lambda_2 & 0 \\ 0 & 0 & \lambda_3 \end{pmatrix} U^T. \quad (3)$$

with

$$\lambda_1 = m_1 e^{2i\rho}, \quad \lambda_2 = m_2 e^{2i\sigma}, \quad \lambda_3 = m_3. \quad (4)$$

In this parametrization, the mass matrix elements are given by:

$$\begin{aligned} M_{\nu 11} &= m_1 c_x^2 c_z^2 e^{2i\rho} + m_2 s_x^2 c_z^2 e^{2i\sigma} + m_3 s_z^2, \\ M_{\nu 12} &= m_1 \left(-c_z s_z c_x^2 s_y e^{2i\rho} - c_z c_x s_x c_y e^{i(2\rho-\delta)} \right) + m_2 \left(-c_z s_z s_x^2 s_y e^{2i\sigma} + c_z c_x s_x c_y e^{i(2\sigma-\delta)} \right) + m_3 c_z s_z s_y, \\ M_{\nu 13} &= m_1 \left(-c_z s_z c_x^2 c_y e^{2i\rho} + c_z c_x s_x s_y e^{i(2\rho-\delta)} \right) + m_2 \left(-c_z s_z s_x^2 c_y e^{2i\sigma} - c_z c_x s_x s_y e^{i(2\sigma-\delta)} \right) + m_3 c_z s_z c_y, \\ M_{\nu 22} &= m_1 \left(c_x s_z s_y e^{i\rho} + c_y s_x e^{i(\rho-\delta)} \right)^2 + m_2 \left(s_x s_z s_y e^{i\sigma} - c_y c_x e^{i(\sigma-\delta)} \right)^2 + m_3 c_z^2 s_y^2, \\ M_{\nu 33} &= m_1 \left(c_x s_z c_y e^{i\rho} - c_y s_x e^{i(\rho-\delta)} \right)^2 + m_2 \left(s_x s_z c_y e^{i\sigma} + s_y c_x e^{i(\sigma-\delta)} \right)^2 + m_3 c_z^2 c_y^2, \\ M_{\nu 23} &= m_1 \left(c_x^2 c_y s_y s_z^2 e^{2i\rho} + s_z c_x s_x (c_y^2 - s_y^2) e^{i(2\rho-\delta)} - c_y s_y s_x^2 e^{2i(\rho-\delta)} \right) \\ &\quad + m_2 \left(s_x^2 c_y s_y s_z^2 e^{2i\sigma} + s_z c_x s_x (s_y^2 - c_y^2) e^{i(2\sigma-\delta)} - c_y s_y c_x^2 e^{2i(\sigma-\delta)} \right) + m_3 s_y c_y c_z^2. \end{aligned} \quad (5)$$

Note that under the transformation given by

$$T_1 : \quad \theta_y \rightarrow \frac{\pi}{2} - \theta_y \quad \text{and} \quad \delta \rightarrow \delta \pm \pi, \quad (6)$$

the mass matrix elements are transformed amongst themselves by swapping the indices 2 and 3 and keeping the index 1 intact:

$$\begin{aligned} M_{\nu 11} &\leftrightarrow M_{\nu 11}, & M_{\nu 12} &\leftrightarrow M_{\nu 13} \\ M_{\nu 22} &\leftrightarrow M_{\nu 33}, & M_{\nu 23} &\leftrightarrow M_{\nu 23}. \end{aligned} \quad (7)$$

On the other hand, the mass matrix is transformed into its complex conjugate i.e

$$M_{\nu ij}(T_2(\delta, \rho, \sigma)) = M_{\nu ij}^*((\delta, \rho, \sigma)) \quad (8)$$

under the mapping given by:

$$T_2 : \rho \rightarrow \pi - \rho, \quad \sigma \rightarrow \pi - \sigma, \quad \delta \rightarrow 2\pi - \delta, \quad (9)$$

The above two symmetries $T_{1,2}$ are quite useful in classifying the models and in connecting the phenomenological analysis of patterns related by them.

It is straightforward to relate our parametrization convention Eq. (2) to the more familiar one used in the recent data analysis of [31]. In fact, the mixing angles in the two parameterizations are equal

$$\theta_x \equiv \theta_{12}, \quad \theta_y \equiv \theta_{23}, \quad \theta_z \equiv \theta_{13}. \quad (10)$$

whereas there is a simple linear relation, discussed in [20, 32], between the phases defined in our parametrization and those corresponding to the standard one.

The solar and atmospheric neutrino mass-squared differences are characterized by two independent neutrino mass-squared differences[31]:

$$\delta m^2 \equiv m_2^2 - m_1^2, \quad |\Delta m^2| \equiv \left| m_3^2 - \frac{1}{2}(m_1^2 + m_2^2) \right|, \quad (11)$$

whereas the parameter

$$R_\nu \equiv \frac{\delta m^2}{|\Delta m^2|}. \quad (12)$$

characterizes the hierarchy of these two quantities.

The neutrino mass scales are constrained in the reactor nuclear experiments on beta-decay kinematics and neutrinoless double-beta decay by two parameters which are the effective electron-neutrino mass:

$$\langle m \rangle_e = \sqrt{\sum_{i=1}^3 (|V_{ei}|^2 m_i^2)}, \quad (13)$$

and the effective Majorana mass term $\langle m \rangle_{ee}$:

$$\langle m \rangle_{ee} = |m_1 V_{e1}^2 + m_2 V_{e2}^2 + m_3 V_{e3}^2| = |M_{\nu 11}|. \quad (14)$$

Another parameter with an upper bound coming from cosmological observations is the ‘sum’ parameter Σ :

$$\Sigma = \sum_{i=1}^3 m_i. \quad (15)$$

Moreover, the Jarlskog rephasing invariant quantity is given by[33]:

$$J = s_x c_x s_y c_y s_z c_z^2 \sin \delta \quad (16)$$

There are no experimental bounds on the phase angles, and we take the principal value range for $\delta, 2\rho$ and 2σ to be $[0, 2\pi]$. As to the other oscillation parameters, the experimental constraints give the values stated in Table (1) with 1, 2, and 3- σ errors [31, 34]. Actually, the fits of oscillation data found in [31] and [34] are consistent with each other except that the latter fits are stricter for θ_z . In our numerical analysis, we prefer to use the former fit having a wider range for θ_z in order to easily catch the pattern of variation depending on θ_z . Other groups [35, 36] have also carried out global fits for the oscillation data and their findings are in line with those of the group of [31].

Parameter	Best fit	1 σ range	2 σ range	3 σ range
$\delta m^2 (10^{-5} \text{eV}^2)$	7.58	[7.32, 7.80]	[7.16, 7.99]	[6.99, 8.18]
$ \Delta m^2 (10^{-3} \text{eV}^2)$	2.35	[2.26, 2.47]	[2.17, 2.57]	[2.06, 2.67]
θ_x	33.58 $^\circ$	[32.96 $^\circ$, 35.00 $^\circ$]	[31.95 $^\circ$, 36.09 $^\circ$]	[30.98 $^\circ$, 37.11 $^\circ$]
θ_y	40.40 $^\circ$	[38.65 $^\circ$, 45.00 $^\circ$]	[36.87 $^\circ$, 50.77 $^\circ$]	[35.67 $^\circ$, 53.13 $^\circ$]
θ_z	8.33 $^\circ$	[7.71 $^\circ$, 10.30 $^\circ$]	[6.29 $^\circ$, 11.68 $^\circ$]	[4.05 $^\circ$, 12.92 $^\circ$]
	8.99 $^\circ$	(8.45 $^\circ$, 9.39 $^\circ$)	(7.99 $^\circ$, 9.82 $^\circ$)	(7.47 $^\circ$, 10.80 $^\circ$)
R_ν	0.0323	[0.0296, 0.0345]	[0.0279, 0.0368]	[0.0262, 0.0397]

Table 1: The global-fit results of three neutrino mixing angles ($\theta_x, \theta_y, \theta_z$) and two neutrino mass-squared differences δm^2 and Δm^2 as defined in Eq. (11). The results $[\dots]$ and (\dots) as respectively extracted from [31] and [34]. In [31], it is assumed that $\cos \delta = \pm 1$ and that new reactor fluxes have been used, while in [34] δ is not restricted and the old reactor flux is used.

We adopt the less conservative 2- σ range as reported in [37] for the non oscillation parameters $\langle m \rangle_e$, Σ , whereas for the other non-oscillation parameter $\langle m \rangle_{ee}$ we use values found in [38]:

$$\begin{aligned} \langle m \rangle_e &< 1.8 \text{ eV}, \\ \Sigma &< 1.19 \text{ eV}, \\ \langle m \rangle_{ee} &< 0.34 - 0.78 \text{ eV}. \end{aligned} \quad (17)$$

3 The μ - τ symmetry and neutrino mass matrix

The μ - τ symmetry can be described by the following general set of conditions[22],

$$|V_{\mu i}| = |V_{\tau i}|, \quad \text{for } i = 1, 2, 3. \quad (18)$$

According to our adopted parameterizations for V in Eq.(2) these conditions imply two classes of solutions. The first class, hereafter labeled by class I, is characterized by,

$$\theta_y = \frac{\pi}{4}, \quad 2 s_x c_x s_z c_\delta = 0, \quad (19)$$

while the second class, hereafter labeled by class II, is determined by,

$$\theta_z = \frac{\pi}{2}, \quad s_{2x} s_{2y} c_\delta = c_{2y} c_{2x}, \quad (20)$$

The two classes, I and II, are distinguished by the possible allowed values for mixing angles θ_y and θ_z . In class I, the mixing angle θ_y is fixed to be $\frac{\pi}{4}$, while for class II the mixing angle θ_z is fixed to be $\frac{\pi}{2}$. These restrictions are the only nontrivial consequence of the μ - τ symmetry. Regarding the other mixing angles and phases for each class, the restriction imposed through the symmetry is rather loose. However, according to the allowed values for mixing angles and phases, the class II cannot be divided into a finite number of sub-classes in contrast to the class I which can be divided into four sub-classes as follows,

- (a) $\theta_y = \frac{\pi}{4}$ and $\theta_x = 0$ while θ_z, δ, ρ and σ are free,
- (b) $\theta_y = \frac{\pi}{4}$ and $\theta_x = \frac{\pi}{2}$ while θ_z, δ, ρ and σ are free,
- (c) $\theta_y = \frac{\pi}{4}$ and $\theta_z = 0$ while θ_x, δ, ρ and σ are free,
- (d) $\theta_y = \frac{\pi}{4}$ and $\delta = \pm \frac{\pi}{2}$ while θ_x, θ_z, ρ and σ are free.

The sub-classes (a) and (b) seem unsatisfactory because the predicted θ_x is far from the experimentally preferred value. The remedy for this defect is to introduce a small perturbation having a large effect on θ_x as was done in [22]. As to the sub-class (c), it seems to be the most interesting class, from a phenomenological point of view, when joint by fixing θ_x near the experimentally preferred value. In a sense, it can contain models with tri-bimaximal, bimaximal, hexagonal, and A_5 symmetries. The last remaining sub-class (d), predicting maximal CP violation, can include the tetramaximal symmetry [39]. The class II is phenomenologically disfavored since $\theta_z = \frac{\pi}{2}$ is far from the experimentally preferred value, which might justify dropping this whole class in the analysis carried out in[22].

We can get more insight into the μ - τ symmetry by writing its implications on the neutrino mass matrix entries. The class I and its sub-classes are found to imply

- (a) $M_{\nu 12} = M_{\nu 13}$ and $M_{\nu 22} = M_{\nu 33}$,
- (b) $M_{\nu 12} = M_{\nu 13}$ and $M_{\nu 22} = M_{\nu 33}$,
- (c) $M_{\nu 12} = -M_{\nu 13}$ and $M_{\nu 22} = M_{\nu 33}$,
- (d) $M_{\nu 12} = M_{\nu 13}^*$ and $M_{\nu 22} = M_{\nu 33}^*$ for vanishing Majorana phases, otherwise no simple algebraic relation between the mass entries is found.

In the second class II, the implied mass relations are,

$$M_{\nu 12} = M_{\nu 13} = 0, \text{ and } |M_{\nu 22}| = |M_{\nu 33}|. \quad (21)$$

The above mentioned considerations motivate us to take as a starting point one of the following mass relations as defining the μ - τ symmetry. The first relation is taken to be

$$M_{\nu 12} = M_{\nu 13}, \text{ and } M_{\nu 22} = M_{\nu 33}. \quad (22)$$

while the second one is

$$M_{\nu 12} = -M_{\nu 13}, \text{ and } M_{\nu 22} = M_{\nu 33}. \quad (23)$$

These two alternative ways for imposing $\mu-\tau$ symmetry in Eq.(22) and Eq.(23) are respectively designated by S_+ and S_- in order to ease the corresponding referral. The other possible relations like $(M_{\nu 12} = M_{\nu 13}^*$ and $M_{\nu 22} = M_{\nu 33}^*)$ or $(M_{\nu 12} = M_{\nu 13} = 0$ and $|M_{\nu 22}| = |M_{\nu 33}|)$ are disfavored because they involve non analytical algebraic relation between mass entries that cannot be generated by usual discrete flavor symmetries. There is still a further motivation for imposing $\mu-\tau$ symmetry via S_+ or S_- which can be easily inferred from the symmetry properties enjoyed by the neutrino mass matrix as explained in section 2. In fact, the transformation rule in Eq.(6) singles out $\theta = \frac{\pi}{4}$ as a fixed point for the transformation and the mass relations in Eq.(7) already links the mass matrix entries relevant for the $\mu-\tau$ symmetry. The difference in sign between the two alternative realizations, $M_{\nu 12} = \pm M_{\nu 13}$, can be attributed to the different phases assigned to the third neutrino filed ν_τ .

4 The exact $\mu-\tau$ symmetry as a texture for non singular neutrino mass matrix

The exact exact $\mu-\tau$ symmetry can be treated as a texture defined by,

$$\begin{aligned} M_{\nu 12} \mp M_{\nu 13} &= 0, \\ M_{\nu 22} - M_{\nu 33} &= 0, \end{aligned} \quad (24)$$

where the minus and plus sign correspond respectively to the cases of Eq.(22) and Eq.(23).

Using Eqs. (2-4), the relation defining the texture can be expressed as

$$\begin{aligned} M_{\nu 12} \mp M_{\nu 13} = 0, &\Rightarrow \sum_{j=1}^3 (U_{1j} U_{2j} \mp U_{1j} U_{3j}) \lambda_j = 0 \\ &\Rightarrow A_1^\mp \lambda_1 + A_2^\mp \lambda_2 + A_3^\mp \lambda_3 = 0 \\ M_{\nu 22} - M_{\nu 33} = 0, &\Rightarrow \sum_{j=1}^3 (U_{2j} U_{2j} - U_{3j} U_{3j}) \lambda_j = 0, \\ &\Rightarrow B_1 \lambda_1 + B_2 \lambda_2 + B_3 \lambda_3 = 0 \end{aligned} \quad (25)$$

where

$$A_j^\mp = U_{1j} (U_{2j} \mp U_{3j}), \quad \text{and} \quad B_j = U_{2j}^2 - U_{3j}^2, \quad (\text{no sum over } j). \quad (26)$$

The coefficients A^\mp and B can be written explicitly in terms of mixing angles and Dirac phase as,

$$\begin{aligned} A_1^\mp &= -c_x c_z [c_x s_z (s_y \mp c_y) + s_x (c_y \pm s_y) e^{-i\delta}], \\ B_1 &= (c_x s_y s_z + s_x c_y e^{-i\delta})^2 - (-c_x c_y s_z + s_x s_y e^{-i\delta})^2, \\ A_2^\mp &= -s_x c_z [s_x s_z (s_y \mp c_y) \mp c_x (s_y \pm c_y) e^{-i\delta}], \\ B_2 &= (-s_x s_y s_z + c_x c_y e^{-i\delta})^2 - (s_x c_y s_z + c_x s_y e^{-i\delta})^2, \\ A_3^\mp &= s_z c_z (s_y \mp c_y), \\ B_3 &= c_z^2 (s_y^2 - c_y^2). \end{aligned} \quad (27)$$

Provided λ_3 is non-vanishing, the equations (25) can be treated as two inhomogeneous linear equations of the ratios $\frac{\lambda_1}{\lambda_3}$ and $\frac{\lambda_2}{\lambda_3}$ which can be solved to get,

$$\begin{aligned} \frac{\lambda_1}{\lambda_3} &= \frac{A_3^\mp B_2 - A_2^\mp B_3}{A_2^\mp B_1 - A_1^\mp B_2}, \\ \frac{\lambda_2}{\lambda_3} &= \frac{A_1^\mp B_3 - A_3^\mp B_1}{A_2^\mp B_1 - A_1^\mp B_2}. \end{aligned} \quad (28)$$

Computing the mass spectrum, we find that it is always a degenerate one ($m_1 = m_2 = m_3$) leading to vanishing mass-squared differences, which is unacceptable phenomenologically. Explicitly, for the cases (a) to (c) mentioned in the previous section and respecting exact $\mu-\tau$ symmetry, we have all the coefficients A^\mp 's and B 's vanishing except: $A_3^+ = -A_1^+ = s_z c_z$ (case a), $A_3^+ = -A_2^+ = s_z c_z$ (case b) and $A_1^- = -A_2^- = -\sqrt{2} s_x c_x e^{-i\delta}$ (case c).

5 The exact $\mu - \tau$ symmetry as a texture for singular neutrino mass matrix

One may wonder that our analysis might lead to non trivial results for singular neutrino mass matrix. Thus, it is crucial to carry the same study for singular case, and keep in mind that the viable singular neutrino mass matrices have to be characterized by vanishing m_1 or m_3 . The vanishing of m_2 leading to the simultaneous vanishing of m_1 and m_2 is not at all phenomenologically consistent.

	$m_1 = 0$	
Realization	$\frac{m_2}{m_3}$	
S_-	$\left \frac{A_3^-}{A_2^-} \right \approx \sqrt{\frac{1-s_{2y}}{1+s_{2y}}} \frac{s_z}{s_x c_x} + O(s_z^2)$	$\left \frac{B_3}{B_2} \right \approx \frac{1}{c_x^2} (1 + 2 t_x t_{2y} c_\delta s_z) + O(s_z^2)$
S_+	$\left \frac{A_3^+}{A_2^+} \right \approx \sqrt{\frac{1+s_{2y}}{1-s_{2y}}} \frac{s_z}{s_x c_x} + O(s_z^2)$	$\left \frac{B_3}{B_2} \right \approx \frac{1}{c_x^2} (1 + 2 t_x t_{2y} c_\delta s_z) + O(s_z^2)$
	$m_3 = 0$	
Realization	$\frac{m_2}{m_1}$	
S_-	$\left \frac{A_1^-}{A_2^-} \right \approx 1 - \frac{(1-s_{2y}) c_\delta s_z}{c_{2y} s_x c_x} + O(s_z^2)$	$\left \frac{B_1}{B_2} \right \approx t_x^2 \left(1 + \frac{2 t_{2y} c_\delta s_z}{s_x c_x} \right) + O(s_z^2)$
S_+	$\left \frac{A_1^+}{A_2^+} \right \approx 1 + \frac{(1+s_{2y}) c_\delta s_z}{c_{2y} s_x c_x} + O(s_z^2)$	$\left \frac{B_1}{B_2} \right \approx t_x^2 \left(1 + \frac{2 t_{2y} c_\delta s_z}{s_x c_x} \right) + O(s_z^2)$

Table 2: The approximate mass ratio formulae for the singular light neutrino mass realizing exact $\mu - \tau$ symmetry. The formulae are calculated in terms of A's or B's coefficients

5.1 Vanishing m_1 singular neutrino mass matrix having exact $\mu - \tau$ symmetry

The mass spectrum in this case turns out to be,

$$m_1 = 0, \quad m_2 = \sqrt{\delta m^2}, \quad m_3 = \sqrt{\Delta m^2 + \frac{\delta m^2}{2}} \approx \sqrt{\Delta m^2}, \quad (29)$$

which puts the mass ratio $\frac{m_2}{m_3}$ in the form

$$m_{23} \equiv \frac{m_2}{m_3} = \sqrt{\frac{R_\nu}{1 + \frac{R_\nu}{2}}} \approx \sqrt{R_\nu}, \quad (30)$$

where the phenomenologically acceptable value for R_ν is given in Table (1). The vanishing of m_1 together with imposing the exact $\mu - \tau$ symmetry as stated in Eqs.(25) leads to,

$$\begin{aligned} A_2^\mp \lambda_2 + A_3^\mp \lambda_3 &= 0, \\ B_2 \lambda_2 + B_3 \lambda_3 &= 0, \end{aligned} \quad (31)$$

which gives non trivial solutions, provided $A_2^\mp B_3 - A_3^\mp B_2 = 0$, i.e.

$$m_{23} = \left| \frac{A_3^\mp}{A_2^\mp} \right| = \left| \frac{B_3}{B_2} \right|, \quad \sigma = \frac{1}{2} \text{Arg} \left(-\frac{A_3^\mp m_3}{A_2^\mp m_2} \right) = \frac{1}{2} \text{Arg} \left(-\frac{B_3 m_3}{B_2 m_2} \right). \quad (32)$$

The Majorana phase ρ becomes unphysical, since m_1 vanishes, in this case, and can be dropped out.

These patterns can be easily shown to be unviable just by comparing the two approximate expressions obtained for $\frac{m_2}{m_3}$. As an example we consider the case S_- where we have, as reported in Table (2),

$$m_{23} \approx \begin{cases} \sqrt{\frac{1-s_{2y}}{1+s_{2y}}} \frac{s_z}{s_x c_x} + O(s_z^2), & \text{from } A^- \text{'s}, \\ \frac{1}{c_x^2} (1 + 2 t_x t_{2y} c_\delta s_z) + O(s_z^2), & \text{from } B \text{'s}, \end{cases} \quad (33)$$

This mass ratio, $\frac{m_2}{m_3}$ should be consistent with the constraint of Eq. (30), which means that it should be much less than one. It is hard to satisfy this constraint because the first expression, obtained from A^- 's, starts from $O(s_z)$ and can be tuned to a small value, while the second one, obtained from B 's, has a leading contribution ($\frac{1}{c_x^2}$) which is greater than one for the admissible range of θ_x . To properly tune the second expression, one needs large negative higher order corrections which can be achieved by choosing negative c_δ and letting θ_y approach $\frac{\pi}{4}$, but this tends in its turn to diminish the first expression of the mass ratio more than required. Thus, the two expression cannot be made compatible. A similar reasoning can be applied to the case S_+ to show the incompatibility of the two derived expressions for the mass ratio. Our numerical study confirms this conclusion where all the phenomenologically acceptable ranges for mixing angles and Dirac phase are scanned, but no solutions could be found satisfying the mass constraint expressed in Eq. (30)

5.2 Vanishing m_3 singular neutrino mass matrix having exact $\mu - \tau$ symmetry

Along the same lines of the previous subsection, we can treat the case of vanishing m_3 . This time, the mass spectrum is found to be,

$$m_1 = \sqrt{\Delta m^2 - \frac{\delta m^2}{2}}, \quad m_2 = \sqrt{\Delta m^2 + \frac{\delta m^2}{2}}, \quad m_3 = 0, \quad (34)$$

forcing the mass ratio $\frac{m_2}{m_1}$ to be

$$m_{21} \equiv \frac{m_2}{m_1} = \sqrt{\frac{1 + \frac{R_\nu}{2}}{1 - \frac{R_\nu}{2}}} \approx 1 + \frac{R_\nu}{2} \gtrsim 1. \quad (35)$$

The vanishing of m_3 together with imposing exact $\mu - \tau$ symmetry as stated in Eqs.(25) result in the following equations,

$$\begin{aligned} A_1^\mp \lambda_1 + A_2^\mp \lambda_2 &= 0, \\ B_1 \lambda_1 + B_2 \lambda_2 &= 0, \end{aligned} \quad (36)$$

which have non trivial solutions as,

$$m_{21} = \left| \frac{A_1^\mp}{A_2^\mp} \right| = \left| \frac{B_1}{B_2} \right|, \quad \rho - \sigma = \frac{1}{2} \text{Arg} \left(-\frac{A_2^\mp m_2}{A_1^\mp m_1} \right) = \frac{1}{2} \text{Arg} \left(-\frac{B_2 m_2}{B_1 m_1} \right), \quad (37)$$

provided $A_1^\mp B_2 - A_2^\mp B_1 = 0$. It is clear that the only relevant physical combination of Majorana phases in such a case is the difference $\rho - \sigma$. One can use the same reasoning explained in the case of vanishing m_1 , based on approximate formulae for mass ratios, as reported in Table (2), to show that the constraint of Eq. 35 cannot be satisfied, which makes the patterns unviable. Again, our numerical study based on scanning all phenomenologically acceptable ranges for mixing angles and Dirac phase reveals no solutions found satisfying the constraint of Eq. (35).

Our investigations, which are so far model independent, point out that imposing exact $\mu - \tau$ symmetry always produces phenomenologically unsatisfactory results. Thus one might find the solace by demanding violation of the exact $\mu - \tau$ symmetry. In breaking the symmetry, we are going to try the simplest and minimal ways of breaking.

6 Deviation from exact $\mu-\tau$ symmetry

We consider the simplest minimal possible deviation from the exact $\mu-\tau$ symmetry that can be parameterized by only one parameter. The relations characterizing these deviations can assume the following two forms,

$$M_{\nu 12} (1 + \chi) = \pm M_{\nu 13}, \text{ and } M_{\nu 22} = M_{\nu 33}, \quad (38)$$

and

$$M_{\nu 12} = \pm M_{\nu 13}, \text{ and } M_{\nu 22} (1 + \chi) = M_{\nu 33}, \quad (39)$$

where $\chi = |\chi| e^{i\theta}$ is a complex parameter measuring the deviation from exact $\mu-\tau$ symmetry. The absolute value $|\chi|$ is restricted to fall in the range $[0, 0.2]$, while the phase θ is totally free. The chosen range for χ is made to ensure a small deviation that can be treated as a perturbation.

The deviation from exact $\mu-\tau$ symmetry can be treated in an illuminating way by considering the relations in Eqs.(38,39) as defining the following textures

$$M_{\nu 12} (1 + \chi) \mp M_{\nu 13} = 0, \text{ and } M_{\nu 22} - M_{\nu 33} = 0, \quad (40)$$

and

$$M_{\nu 12} \mp M_{\nu 13} = 0, \text{ and } M_{\nu 22} (1 + \chi) - M_{\nu 33} = 0. \quad (41)$$

Following the same procedure as described in section 4, we find that the coefficients A 's and B 's corresponding to the textures defined in Eq.(40) and Eq.(41) are respectively,

$$A_j^\mp = U_{1j} [U_{2j} (1 + \chi) \mp U_{3j}], \text{ and } B_j = U_{2j}^2 - U_{3j}^2, \quad (\text{no sum over } j). \quad (42)$$

and

$$A_j^\mp = U_{1j} (U_{2j} \mp U_{3j}), \text{ and } B_j = U_{2j}^2 (1 + \chi) - U_{3j}^2, \quad (\text{no sum over } j). \quad (43)$$

Assuming $\lambda_3 \neq 0$, the resulting λ 's ratio are found to be,

$$\begin{aligned} \frac{\lambda_1}{\lambda_3} &= \frac{A_3 B_2 - A_2 B_3}{A_2 B_1 - A_1 B_2}, \\ \frac{\lambda_2}{\lambda_3} &= \frac{A_1 B_3 - A_3 B_1}{A_2 B_1 - A_1 B_2}, \end{aligned} \quad (44)$$

From these λ -ratios, the mass ratios $\left(\frac{m_1}{m_3}, \frac{m_2}{m_3}\right)$ and Majorana phases (ρ, σ) can be determined in terms of the mixing angles $((\theta_x, \theta_y, \theta_z))$, the Dirac phase δ and the complex parameter χ . Thus, we can vary $(\theta_x, \theta_y, \theta_z, \delta m^2)$ over their experimentally allowed regions and $(\delta, |\chi|, \theta)$ in their full range to determine the unknown mass spectra and Majorana phases. We can then confront the whole predictions with the experimental constraints given in Table (1) and Eq. (17) to find out the admissible 7-dim parameter space region. For a proper survey of the allowed parameter space, one can illustrate graphically all the possible correlations, at the three levels of σ -error, between any two physical neutrino parameters. We chose to plot for each pattern and for each type of hierarchy thirty four correlations at the $3\text{-}\sigma$ error level involving the parameters $(m_1, m_2, m_3, \theta_x, \theta_y, \theta_z, \rho, \sigma, \delta, J, m_{ee}, |\chi|, \theta)$ and the lowest neutrino mass (**LNM**). Moreover, for each parameter, one can determine the extremum values it can take according to the considered precision level, and we listed in tables these predictions for all the patterns and for the three σ -error levels.

The resulting mass patterns are found to be classifiable into three categories:

- Normal hierarchy: characterized by $m_1 < m_2 < m_3$ and is denoted by **N** satisfying numerically the bound:

$$\frac{m_1}{m_3} < \frac{m_2}{m_3} < 0.7 \quad (45)$$

- Inverted hierarchy: characterized by $m_3 < m_1 < m_2$ and is denoted by **I** satisfying the bound:

$$\frac{m_2}{m_3} > \frac{m_1}{m_3} > 1.3 \quad (46)$$

- Degenerate hierarchy (meaning quasi- degeneracy): characterized by $m_1 \approx m_2 \approx m_3$ and is denoted by **D**. The corresponding numeric bound is taken to be:

$$0.7 < \frac{m_1}{m_3} < \frac{m_2}{m_3} < 1.3 \quad (47)$$

Moreover, we studied for each pattern the possibility of having a singular (non-invertible) mass matrix characterized by one of the masses (m_1 , and m_3) being equal to zero (the data prohibits the simultaneous vanishing of two masses and thus m_2 can not vanish).

7 Numerical results of various patterns violating exact $\mu - \tau$ symmetry

We present now the results of our numerical analysis for the four simplest possible patterns violating exact $\mu - \tau$ as described in the previous section and quantified in Eq.(40) and Eq.(41). The coefficients A 's and B 's are expressed in Eq.(42) and Eq.(43) according to the pattern under study. Moreover, analytical expressions of the relevant parameters up to leading order in s_z are provided in order to get an “understanding” of the numerical results. The relevant parameters include mass ratios, Majorana phases, R_ν parameter, effective Majorana mass term $\langle m \rangle_{ee}$ and effective electron's neutrino mass $\langle m \rangle_e$. We stress here that our numerical analysis is based on the exact formulae and not on the approximate ones.

The large number of correlation figures is organized in plots, at the $3\text{-}\sigma$ -error level, by dividing each figure into left and right panels (halves) denoted accordingly by the letters L and R. Additional labels (D, N and I) are attached to the plots to indicate the type of hierarchy (Degenerate, Normal and Inverted, respectively). Any missing label D, N or I on the figures of certain pattern means the absence of the corresponding hierarchy type in this pattern.

We list in tables (3) and (4), and for the three types of hierarchy and the three precision levels, the extremum values that the different parameters can take. It is noteworthy that our numerical study is based, as was the case in [32], on random scanning of the 7-dim parameter space composed of $(\theta_x, \theta_y, \theta_z, \delta, \delta m^2, |\chi|$ and $\theta)$. This kind of randomness implies that the reported values in the tables are meant to give only a strong qualitative indication, in that they might change from one run to another, providing thus a way to check for the stability of the results.

7.1 C1: Pattern having $M_{\nu 12} (1 + \chi) - M_{\nu 13} = 0$, and $M_{\nu 22} - M_{\nu 33} = 0$.

In this pattern, C1, the relevant expressions for A 's and B 's are

$$\begin{aligned} A_1 &= -c_x c_z (c_x s_y s_z + s_x c_y e^{-i\delta}) (1 + \chi) - c_x c_z (-c_x c_y s_z + s_x s_y e^{-i\delta}), \\ A_2 &= s_x c_z (-s_x s_y s_z + c_x c_y e^{-i\delta}) (1 + \chi) + s_x c_z (s_x c_y s_z + c_x s_y e^{-i\delta}), \\ A_3 &= s_z s_y c_z (1 + \chi) - s_z c_y c_z, \\ B_1 &= (c_x s_y s_z + s_x c_y e^{-i\delta})^2 - (-c_x c_y s_z + s_x s_y e^{-i\delta})^2, \\ B_2 &= (-s_x s_y s_z + c_x c_y e^{-i\delta})^2 - (s_x c_y s_z + c_x s_y e^{-i\delta})^2, \\ B_3 &= s_y^2 c_z^2 - c_y^2 c_z^2, \end{aligned} \quad (48)$$

leading to mass ratios, up to leading order in s_z , as

$$\begin{aligned} m_{13} \equiv \frac{m_1}{m_3} &\approx 1 + \frac{2 s_\delta s_\theta |\chi| s_z}{t_x T_1}, \\ m_{23} \equiv \frac{m_2}{m_3} &\approx 1 - \frac{2 t_x s_\delta s_\theta |\chi| s_z}{T_1}, \end{aligned} \quad (49)$$

where T_1 is defined as,

$$T_1 = |\chi|^2 c_y^2 + 2 |\chi| c_\theta c_y (c_y + s_y) + 1 + s_{2y}. \quad (50)$$

While the Majorana phases as,

$$\begin{aligned}\rho &\approx \delta + \frac{s_\delta s_z \left(-s_y c_y |\chi|^2 + |\chi| c_\theta (c_{2y} - s_{2y}) + c_{2y} \right)}{t_x T_1}, \\ \sigma &\approx \delta - \frac{s_\delta t_x s_z \left(-s_y c_y |\chi|^2 + |\chi| c_\theta (c_{2y} - s_{2y}) + c_{2y} \right)}{T_1}.\end{aligned}\quad (51)$$

The parameters R_ν , mass ratio square difference $m_{23}^2 - m_{13}^2$, $\langle m \rangle_e$ and $\langle m \rangle_{ee}$ can be deduced to be,

$$\begin{aligned}R_\nu &\approx -\frac{8 s_\delta s_\theta |\chi| s_z}{s_{2x} T_1}, \\ m_{23}^2 - m_{13}^2 &\approx -\frac{8 s_\delta s_\theta |\chi| s_z}{s_{2x} T_1}, \\ \langle m \rangle_e &\approx m_3 \left[1 + \frac{4 s_\theta s_\delta |\chi| s_z}{t_{2x} T_1} \right], \\ \langle m \rangle_{ee} &\approx m_3 \left[1 + \frac{4 s_\theta s_\delta |\chi| s_z}{t_{2x} T_1} \right].\end{aligned}\quad (52)$$

Our expansion in terms of s_z is justified since s_z is typically small for phenomenologically acceptable values where the best fit for $s_z \approx 0.144$. Therefore, we naively expect that the expansion should work properly but it turns out that there are some subtle points in this expansion which would invalidate our naive expectation. To elaborate on this, let us consider the expansion corresponding to the mass ratio m_{13} as,

$$m_{13} = 1 + \sum_{i=1}^{\infty} c_i (\theta_x, \theta_y, \delta, |\chi|, \theta) s_z^i, \quad (53)$$

where c_i is the i^{th} -Taylor expansion coefficient depending on $\theta_x, \theta_y, \delta, |\chi|$ and θ . In this pattern, putting θ_y equal to $\frac{\pi}{4}$ makes the spectrum degenerate ($m_{13} = m_{23} = 1$) irrespective of the values for $\theta_x, \delta, |\chi|$ and θ . There are two possible alternatives to match this finding: in the first one, all the $c_i (\theta_y = \frac{\pi}{4})$'s are vanishing, whereas in the second one some of the $c_i (\theta_y = \frac{\pi}{4})$'s are finite and non-vanishing provided that an infinite number of $c_i (\theta_y = \frac{\pi}{4})$'s are divergent such that the coefficients recombine in a delicate way to make the sum $\sum_{i=1}^{\infty} c_i (\theta_x, \theta_y = \frac{\pi}{4}, \delta, |\chi|, \theta) s_z^i$ equaling zero for any s_z *. Explicit calculation reveals that c_1 is finite and non vanishing at $\theta_y = \frac{\pi}{4}$ as is evident from Eq.(49), while c_i is divergent at $\theta_y = \frac{\pi}{4}$ for all $i \geq 2$. A similar consideration applies also to the mass ratio m_{23} . These divergences, at $\theta_y = \frac{\pi}{4}$, appearing in the expansion coefficients c_i for mass ratios resurface again in the expansion coefficients corresponding to $\langle m \rangle_e$ and $\langle m \rangle_{ee}$ but surprisingly enough the divergences associated with R_ν and $m_{23}^2 - m_{13}^2$ start only from the third order coefficients. All these subtleties are an artifact of the expansion, whereas no such problems arise if we use exact formulae. Thus, the formulae due to expansion must be dealt with caution.

All the possible fifteen pair correlations related to the three mixing angles and the three Majorana and Dirac phases ($\theta_x, \theta_y, \theta_z, \delta, \rho, \sigma$) are presented in the left and right panels of Figure 1, while the last plot in the right panel is reserved for the correlation of m_{23} against θ_y .

In Fig. 2, left panel, we present five correlations of J against ($\theta_z, \delta, \sigma, \rho$ and **LN**M) and the correlation of ρ versus **LN**M. As to the right panel, we include presentation for the correlations of $\langle m \rangle_{ee}$ against $\theta_x, \theta_z, \rho, \sigma$, **LN**M, and J .

As to Fig. 3, and in a similar way, we present correlations for θ against θ_y and δ and for $|\chi|$ versus θ_y and θ_z . The correlation of m_3 against m_{23} and m_{21} are also included. All correlations are exhibited for all three types of hierarchy and for each type we have thirty four depicted correlations.

*One can see this simply by noting that in case all the c_i 's are bounded then the analyticity of the series forces them to vanish. On the other hand, one can not have a finite number of 'unbounded' expansion coefficients, otherwise we could, assuming without loss of generality two coefficients ($c_{i_1}, c_{i_2}, i_1 < i_2$) whose limits at $y = y_0 = \frac{\pi}{4}$ are divergent, write $c_{i_1}(y)t^{i_1} + c_{i_2}(y)t^{i_2} = g(y, t)$ where g is a well behaved function if the infinite sum of 'bounded' terms converge. It suffices

then to let y , for $t_1 \neq t_2$, approach y_0 in the relation $c_{i_2}(y) = \frac{\frac{g(y, t_1)}{t_1^{i_1}} - \frac{g(y, t_2)}{t_2^{i_1}}}{t_1^{i_2-i_1} - t_2^{i_2-i_1}}$ to reach a contradiction.

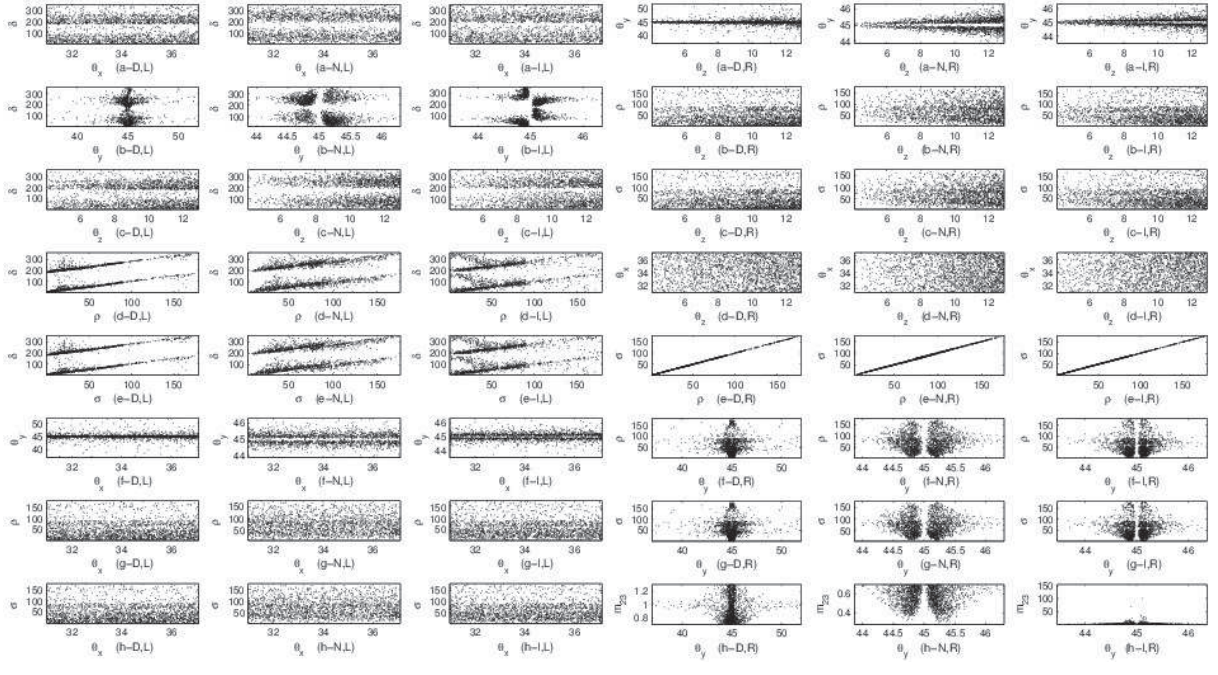


Figure 1: Pattern having $M_{\nu 12} (1 + \chi) - M_{\nu 13} = 0$, and $M_{\nu 22} - M_{\nu 33} = 0$: The left panel (the left three columns) presents correlations of δ against mixing angles and Majorana phases (ρ and σ) and those of θ_x against θ_y , ρ and σ . The right panel (the right three columns) shows the correlations of θ_z against θ_y , ρ , σ , and θ_x and those of ρ against σ and θ_y , and also the correlation of θ_y versus σ and m_{23} .

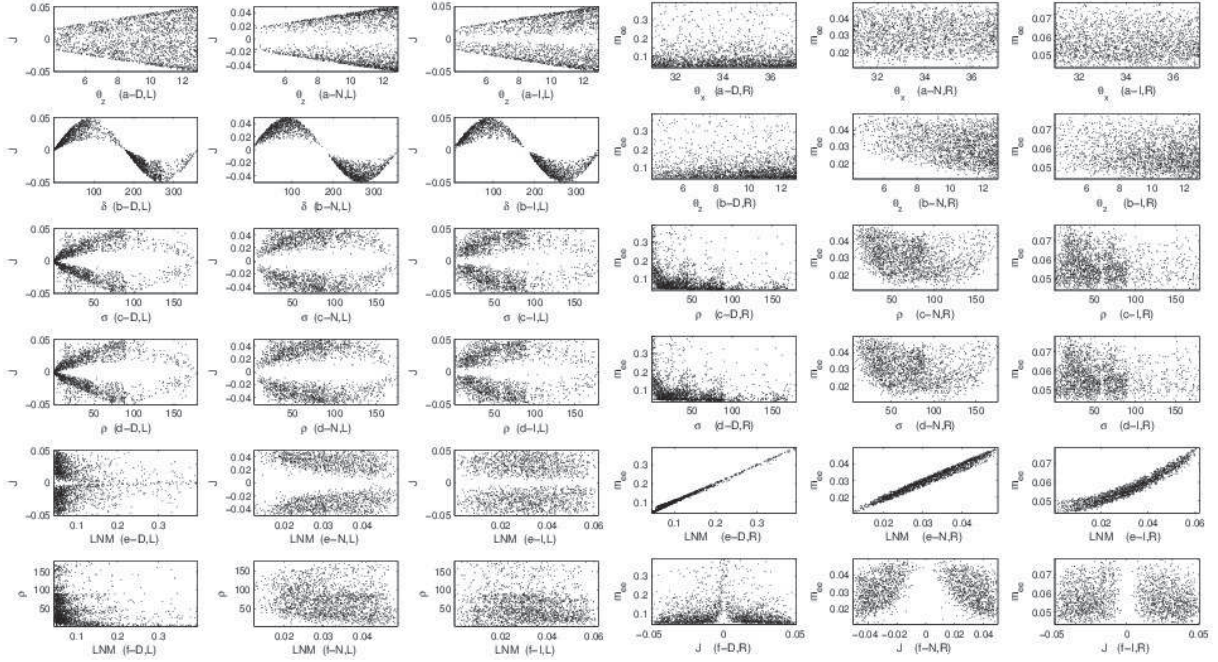


Figure 2: Pattern having $M_{\nu 12} (1 + \chi) - M_{\nu 13} = 0$, and $M_{\nu 22} - M_{\nu 33} = 0$: Left panel presents correlations of J against θ_z , δ , σ , ρ , and lowest neutrino mass (LNM), while the last one depicts the correlation of LNM against ρ . The right panel shows correlations of m_{ee} against θ_x , θ_z , ρ , σ , LNM and J .

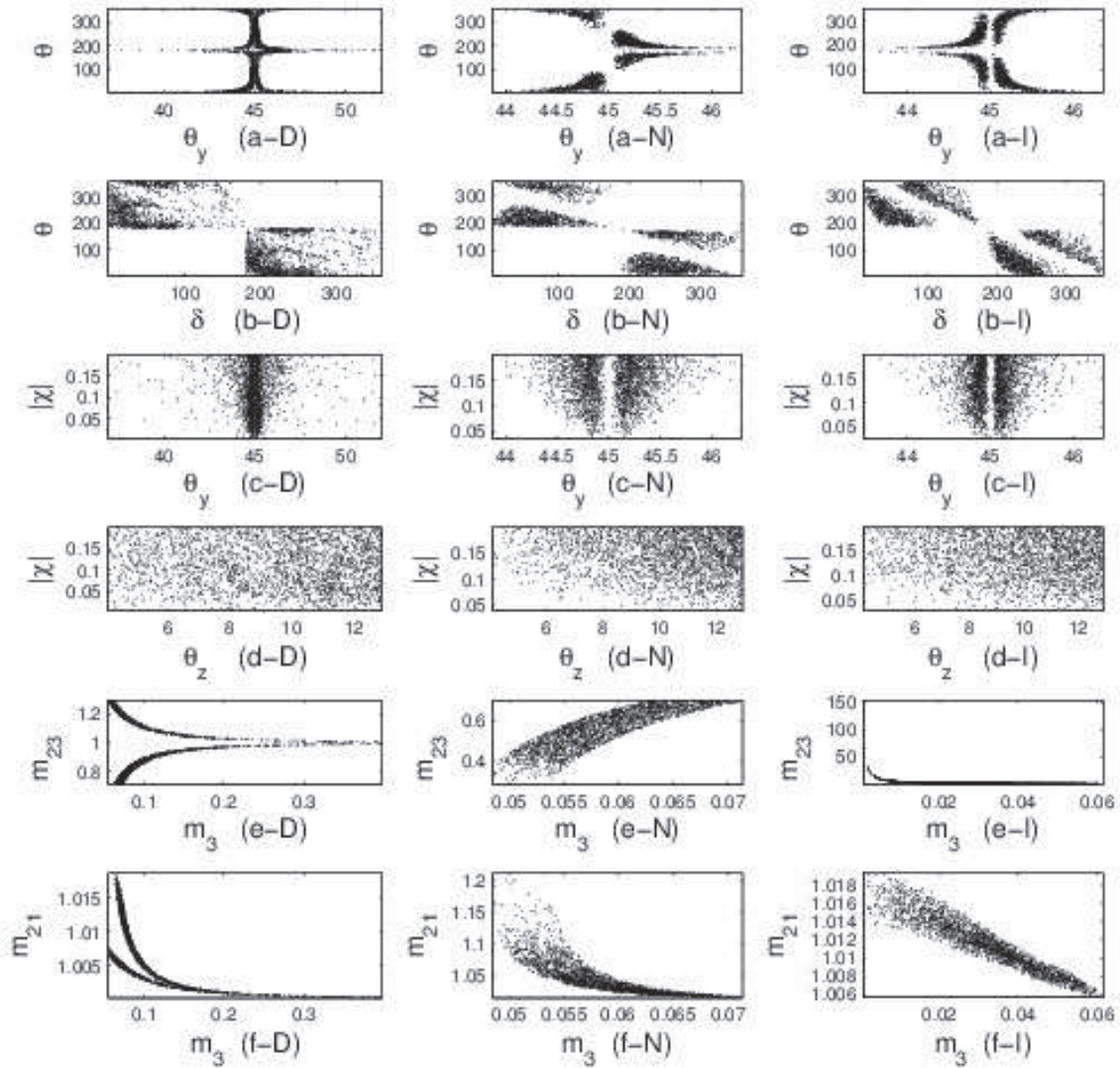


Figure 3: Pattern having $M_{\nu 12}(1 + \chi) - M_{\nu 13} = 0$, and $M_{\nu 22} - M_{\nu 33} = 0$: The first two rows presents the correlations of θ against θ_y and δ , while the second two rows depict those of $|\chi|$ versus θ_y and θ_z . The last two rows shows the correlations of mass ratios m_{23} and m_{21} against m_3 .

Before dwelling into examining the correlations provided by the various figures we can infer some restrictions concerning mixing angles and phases in each pattern just by considering the expression for R_ν as given in Eq.(52). The parameter R_ν must be positive, nonvanishing and at the $3 - \sigma$ level is restricted to be in the interval $[0.0262, 0.0397]$. This clearly requires nonvanishing values for s_z , s_δ , s_θ and $|\chi|$. The nonvanishing of s_z means $\theta_z \neq 0$ which is phenomenologically favorable, while vanishing of s_δ , s_θ implies excluding 0 , π and 2π for both δ and θ . The nonvanishing of $|\chi|$ is naturally expected otherwise there would not be a deviation from exact $\mu - \tau$ symmetry. The other required restriction, namely, $s_\theta s_\delta < 0$ dictates that if δ falls in the first and second quadrants then θ falls in third and fourth quadrants and vice versa. These conclusions remain valid if one used the exact expression for R_ν instead of the first order expression. Explicit computations of R_ν using its exact expression tell us that θ_y cannot be exactly equal to $\frac{\pi}{4}$ otherwise R_ν would be zero, but nevertheless θ_y can possibly stay very close to $\frac{\pi}{4}$.

We see in Fig. 1 (plots: a-L \rightarrow c-L, as examples) that all the experimentally allowed ranges of mixing angles, at 3σ error levels, can be covered in this pattern except for normal and inverted hierarchy types where θ_y is restricted to be around 45° , by at most, plus or minus 1.5° . This restriction on θ_y is a characteristic of the normal and inverted hierarchy type in this pattern. This characteristic behaviour of

θ_y can be understood by expressing the mass ratios, using Eqs. (49, 50 and 52), as

$$\begin{aligned} m_{13} &= 1 - \frac{1}{2} c_x^2 R_\nu + O(s_z^2), \\ m_{23} &= 1 + \frac{1}{2} s_x^2 R_\nu + O(s_z^2), \end{aligned} \quad (54)$$

where the first order correction is identified consistently with R_ν expressed up to this order. All the remaining higher order corrections to the mass ratios contribute significantly and in a spiky way in the vicinity of $\theta_y = \frac{\pi}{4}$ leading to mass ratios considerably greater or smaller than unity. Therefore, to produce the various hierarchy types as marked in Eqs.(45–47), θ_y can take in the degenerate hierarchy type values far from $\frac{\pi}{4}$ corresponding to small higher order corrections in Eq. (54) which would keep m_{13} and m_{23} near the value one. However, in order to get normal or inverted hierarchies, the higher order corrections in Eq. (54) should contribute in a noticeably large amount, which could not be happened unless θ_y stays close to $\frac{\pi}{4}$, and this is what the corresponding ranges for θ_y reported in Table 3 confirm. As to the Dirac CP-phase δ , the whole range is allowed except the regions around 0 and π whose extensions depend on the type of hierarchy and the precision level as evident from the same plots and the reported values in Table 3. Likewise, the plots (g-L, h-L), in Figure 1 and the values reported in Table 3 show that the Majorana phases (ρ, σ) are covering their ranges excluding regions around 0 and π .

The plots in Figure 1 can reveal many obvious clear correlations. For example, the plots (a-R) shows that as θ_z decreases θ_y tends to be very close to 45° . The plots (d-L, e-L) show a sort of distorted linear correlation of δ versus (ρ, σ) in all hierarchy types which confirms the relations presented in Eq. (51) which give linear relations at zeroth order of s_z , while the found distortion can be attributed to the higher order corrections. We may see also also in (plot e-R), a very clear linear correlation between the Majorana phases (ρ, σ) in all hierarchy types which again confirms the relations presented in Eq. (51) which at zeroth order produces the linear relation $\rho \approx \sigma$.

The Figure 2 (plots: a-L, b-L) shows that the correlations (J, θ_z) and (J, δ) have each a specific geometrical shape irrespective of the hierarchy type. In fact, Eq. (16) indicates that the correlation (J, δ) can be seen as a superposition of many sinusoidal graphs in δ , the ‘positive’ amplitudes of which are determined by the acceptable mixing angles, whereas the (J, θ_z) correlation is a superposition of straight-lines in $s_z \sim \theta_z$, for small θ_z , the slopes of which are positive or negative according to the sign of s_δ . The resulting shape for (J, θ_z) correlation being trapezoidal rather than isosceles is due to the exclusion of zero and its vicinity for θ_z considering the latest oscillation data. The unfilled region in the plots originates from the disallowed region of δ around 0 and π , which would have led, if allowed, to zero J .

The left panel of Figure 2 (plots: c-L, d-L), unveils a correlation of J versus (ρ, σ) which is a direct consequence of the ‘linear’ correlations of δ against (ρ, σ) and of the ‘geometrical’ correlation of (J, δ) . The two correlations concerning the **LNM** (plots: e-L, f-L) reveals that as the **LNM** increases the parameter space becomes more restricted. This seems to be a general tendency in all the patterns, where the **LNM** can reach in the degenerate case values higher than in the normal and inverted hierarchies.

To gain more insight about the correlations involving $\langle m \rangle_{ee}$ as defined in Eq. (14), we work out approximate formulae for $\langle m \rangle_{ee}$ corresponding to different hierarchy types. It is helpful in deriving these approximate formulae to realize that $\rho \approx \sigma$ and $m_1 \approx m_2$ in all hierarchy types as is evident respectively from Fig. 1 (plots: e-R) and Fig. 3 (plots: f), and also to realize that the normal hierarchy is moderate (meaning m_3 is of the same order as m_1) while the inverted one is acute as can be inferred from Fig. 3 (plots: e-N, e-I). Thus, the resulting formulae are,

$$\begin{aligned} \langle m \rangle_{ee} &\approx m_1 (1 - 2 s_z^2 c_z^2 s_\sigma^2) && \text{For normal and degenerate cases,} \\ \langle m \rangle_{ee} &\approx m_1 (1 - s_z^2) && \text{For inverted case.} \end{aligned} \quad (55)$$

The correlations of $\langle m \rangle_{ee}$ against $(\theta_x, \theta_z, \rho, \sigma)$ as depicted in the right panel of Fig. 2 (plots: a-R –d-R) can be understood by exploiting the approximate expression for $\langle m \rangle_{ee}$ in conjunction with the correlations found between θ_z and (θ_x, ρ, σ) . The totality of correlations of $\langle m \rangle_{ee}$ presented in the right panel of Fig. 2 indicate that the increase of $\langle m \rangle_{ee}$ would on the whole constrain the allowed parameter space. We note also a general trend of increasing $\langle m \rangle_{ee}$ with increasing **LNM** in all cases of hierarchy (plots e-R). The values of $\langle m \rangle_{ee}$ can not reach the zero-limit in all types of hierarchy, as is evident from the graphs or

explicitly from the corresponding covered range in Table 3. Another point concerning $\langle m \rangle_{ee}$ is that its scale is triggered by the scale of m_1 ($\approx m_2$) as is evident from both the approximate formula in Eq. (55) and the corresponding covered range in Table 3.

The plots in Fig. 3 (plots: b) disclose a clear correlation between θ and δ which is in accordance with what was derived before in that ($s_\theta s_\delta < 0$). The plots also reveal that there are disallowed regions for both θ and δ , which must definitely contain domains around 0 and π besides other possible additional areas. The disallowed regions can be also checked with the help of Tables (3–4) where one additionally finds that the regions around 0 and π tend to be shrunk for the degenerate case. The plots (c) in Fig. 3 show that as θ_y deviates slightly from $\frac{\pi}{4}$ then $|\chi|$ tends to increase.

For the mass spectrum, we see from Fig. 3 (plots: e, f) that the normal hierarchy is mild in that the mass ratios do not reach extreme values. In contrast, the inverted hierarchy can be acute in that the mass ratio m_{23} can reach values up to $O(10^2)$. The values of m_1 and m_2 are nearly equal in all hierarchy types. We also see that if m_3 is large enough then only the degenerate case with $m_1 \sim m_2$ can be phenomenologically acceptable.

7.2 C2: Pattern having $M_{\nu 12} (1 + \chi) + M_{\nu 13} = 0$, and $M_{\nu 22} - M_{\nu 33} = 0$.

In this pattern, C2, the relevant expressions for A 's and B 's are

$$\begin{aligned}
A_1 &= -c_x c_z (c_x s_y s_z + s_x c_y e^{-i\delta}) (1 + \chi) + c_x c_z (-c_x c_y s_z + s_x s_y e^{-i\delta}), \\
A_2 &= s_x c_z (-s_x s_y s_z + c_x c_y e^{-i\delta}) (1 + \chi) - s_x c_z (s_x c_y s_z + c_x s_y e^{-i\delta}), \\
A_3 &= s_z s_y c_z (1 + \chi) + s_z c_y c_z, \\
B_1 &= (c_x s_y s_z + s_x c_y e^{-i\delta})^2 - (-c_x c_y s_z + s_x s_y e^{-i\delta})^2, \\
B_2 &= (-s_x s_y s_z + c_x c_y e^{-i\delta})^2 - (s_x c_y s_z + c_x s_y e^{-i\delta})^2, \\
B_3 &= s_y^2 c_z^2 - c_y^2 c_z^2,
\end{aligned} \tag{56}$$

leading to mass ratios, up to leading order in s_z , as

$$\begin{aligned}
m_{13} &\approx 1 - \frac{2 s_\delta s_\theta |\chi| s_z}{t_x T_2}, \\
m_{23} &\approx 1 + \frac{2 t_x s_\delta s_\theta |\chi| s_z}{T_2},
\end{aligned} \tag{57}$$

where T_2 is defined as,

$$T_2 = |\chi|^2 c_y^2 + 2 |\chi| c_\theta c_y (c_y - s_y) + 1 - s_{2y}. \tag{58}$$

The Majorana phases are given by

$$\begin{aligned}
\rho &\approx \delta - \frac{s_\delta s_z (s_y c_y |\chi|^2 + |\chi| c_\theta (c_{2y} + s_{2y}) + c_{2y})}{t_x T_2}, \\
\sigma &\approx \delta + \frac{s_\delta t_x s_z (s_y c_y |\chi|^2 + |\chi| c_\theta (c_{2y} + s_{2y}) + c_{2y})}{T_2}.
\end{aligned} \tag{59}$$

The parameters R_ν , mass ratio square difference $m_{23}^2 - m_{13}^2$, $\langle m \rangle_e$ and $\langle m \rangle_{ee}$ can be deduced to be,

$$\begin{aligned}
R_\nu &\approx \frac{8 s_\delta s_\theta |\chi| s_z}{s_{2x} T_2}, \\
m_{23}^2 - m_{13}^2 &\approx \frac{8 s_\delta s_\theta |\chi| s_z}{s_{2x} T_2}, \\
\langle m \rangle_e &\approx m_3 \left[1 - \frac{4 s_\theta s_\delta |\chi| s_z}{t_{2x} T_2} \right], \\
\langle m \rangle_{ee} &\approx m_3 \left[1 - \frac{4 s_\theta s_\delta |\chi| s_z}{t_{2x} T_2} \right].
\end{aligned} \tag{60}$$

One can notice that the all results concerning this pattern, C2, can be derived from those of the previous one, C1, by simply making the substitutions $s_y \rightarrow -s_y$ and $\delta \rightarrow \delta + \pi$. Unfortunately, the found relation cannot be used in practice to derive the predictions of one pattern from the other because the mapping $s_y \rightarrow -s_y$ takes θ_y from a physically admissible region to a forbidden one. However, one can also verify that the two patterns have the same properties regarding divergences for the expansion coefficients of the mass ratios.

The approximate expression for R_ν in Eq. (60) provides us with similar restrictions like those of the previous pattern C1, except that both δ and θ should now fall in same upper or lower semicircles. Once again the derived restriction remains unchanged when using the exact expression for R_ν .

We plot the corresponding correlations in Figures (4, 5 and 6) with the same conventions as before. In contrast to the C1 case, we see here that the mixing angle (θ_y) can cover a wider range in the normal and inverted hierarchy cases instead of being confined around $\theta_y = \frac{\pi}{4}$. In the normal hierarchy case θ_y falls in the interval $[41^\circ - 50^\circ]$, while it almost covers all the admissible range in the inverted case. In the degenerate case, however, there is no restriction on θ_y , as it was in the C1 pattern. Another contrasting feature is the range of θ_z in the normal hierarchy type, where it is now restricted to be less than 10° , whereas it can, similarly to the C1 pattern, cover all its allowed range in the inverted and degenerate cases.

We can understand the behaviour of θ_y , compared to that of the previous pattern C1, by expressing the mass ratios, from Eqs. (57,58) and (60), as

$$\begin{aligned} m_{13} &= 1 - \frac{1}{2} c_x^2 R_\nu + O(s_z^2), \\ m_{23} &= 1 + \frac{1}{2} s_x^2 R_\nu + O(s_z^2), \end{aligned} \quad (61)$$

where the first order correction is identified consistently with R_ν expressed up to this order, and thus representing a small quantity. In contrast to the situation in the pattern C1, the remaining higher-order corrections in the mass ratios can be tuned to have a significant contribution in the vicinity of any θ_y depending on the other combinations of mixing angles and phases, which would lead to mass ratios considerably greater or smaller than unity. Therefore the various hierarchy types as marked in Eqs.(45-47) can be generated for almost all θ_y in its allowed range, and the values of θ_y reported in Table 3 confirm this. As to the Dirac CP-phase δ , the whole range is allowed except the regions around 0 and π whose extensions depend on the type of hierarchy and the precision level as is evident from the corresponding plots and from the reported values in Table 3.

The plots in Figure 4 can disclose many obvious clear correlations. For example, the plots (a-R) show, in normal and inverted hierarchy cases, that as θ_z decreases θ_y tends to be spread over its admissible range while the contrary occurs when θ_z increases. The plots (d-L, e-L) do not show a simple correlation of δ versus (ρ, σ) in the various hierarchy types which would have been consistent with the zeroth order linear relation given in Eq. (59). In fact, the higher order corrections bring a severe distortion that invalidate the zeroth order linear relation even at the approximate level. These higher order corrections do not work in the same manner for both ρ and σ , so they do not cancel out upon subtraction producing ambiguous correlation between ρ and σ , as depicted in the (plot e-R), contrasted with the simple linearity in the previous pattern C1. The absence of linear relations among the phases (δ, ρ, σ) forbids the allowed region of Majorana phases to be straightforwardly determined from that of the Dirac phase (δ), as can be figured out looking at the corresponding allowed values in Table 3.

The special ‘sinusoidal’ and ‘trapezoidal’ shapes of J versus δ and θ_z remain intact (Fig. 5, plots: a-L, b-L), and as before the unfilled region in the trapezoidal shaped plots is attributed to the disallowed region for δ around 0 and π . The usual correlations of J versus ρ and σ (Fig. 5 plots: c-L, d-L) emerge from those of δ versus ρ and σ . The two correlations concerning the **LNM** (plots: e-L, f-L) indicate that as the **LNM** increases (say, larger than 0.1 ev) the parameter space becomes more restricted. This seems to represent an inclination in all the patterns, where the **LNM** can reach in the degenerate case values higher than the other hierarchies.

The correlations involving $\langle m \rangle_{ee}$ can be made more transparent by deriving an approximate formula for $\langle m \rangle_{ee}$ capturing the essential observed features for all kinds of hierarchies in this specific pattern C2

which are: first, the equality of m_1 and m_2 as is clear in Fig. 6 (plots: f); second, the mild hierarchy in both normal and inverted cases as is evident from Fig. 6 (plots: e-N, e-I). Thus, one can deduce from Eq. (14) that $\langle m \rangle_{ee}$ is approximated by

$$\langle m \rangle_{ee} \approx m_1 c_z^2 \sqrt{[1 - s_{2x}^2 \sin^2(\rho - \sigma)]}. \quad (62)$$

Now, the correlations of $\langle m \rangle_{ee}$ against $(\theta_x, \theta_z, \rho, \sigma)$ as displayed in the right panel of Figure 5 (plots: a-R –d-R) can be comprehended by invoking the approximate expression for $\langle m \rangle_{ee}$ in conjunction with the pair correlations found amidst θ_x, θ_z, ρ and σ . The whole correlations of $\langle m \rangle_{ee}$ presented in the right panel of Figure 5 point out that the increase of $\langle m \rangle_{ee}$ would generally constrain the allowed parameter space. We note also a general tendency of increasing $\langle m \rangle_{ee}$ with increasing LNM in all cases of hierarchy (plots e-R). The values of $\langle m \rangle_{ee}$ can not attain the zero-limit in all types of hierarchy, as is evident from the graphs or explicitly from the corresponding covered range in Table 3. Another point concerning $\langle m \rangle_{ee}$ is that its scale is triggered by the scale of m_1 ($\approx m_2$) as is evident from both the approximate formula in Eq. (62) and the corresponding covered range stated in Table 3.

The plots in Fig. 6 (plots: b) shows both that θ and δ must lie in the same upper or lower semicircle which confirms our inference based on the approximate formula for R_ν in Eq. (60). The plots also reveal that there are disallowed regions for both θ and δ , which definitely should contain regions around 0 and π besides other possible additional regions. The disallowed regions can be also checked with the help of Tables (3–4) where one can additionally find that the forbidden regions around 0 and π tend to be shrunk for the degenerate case and that the allowed range for θ is very limited in normal and inverted hierarchy. The Figure 6 (plots: c,d) shows that $|\chi|$ tends to increase in normal and inverted heirarchies as θ_y deviates from $\frac{\pi}{4}$ or as θ_z increases.

For the mass spectrum, we see from Fig. 6 (plots: e) that all hierarchy types are characterized by nearly equal values of m_1 and m_2 . Moreover, Fig. 6 (plots: f) reveals that both normal and inverted hierarchies are of moderate type in that the mass ratios m_{23} does not reach extremely low nor high values. We also see that if m_3 is large enough then only the degenerate case with $m_1 \sim m_2$ can be compatible with data.

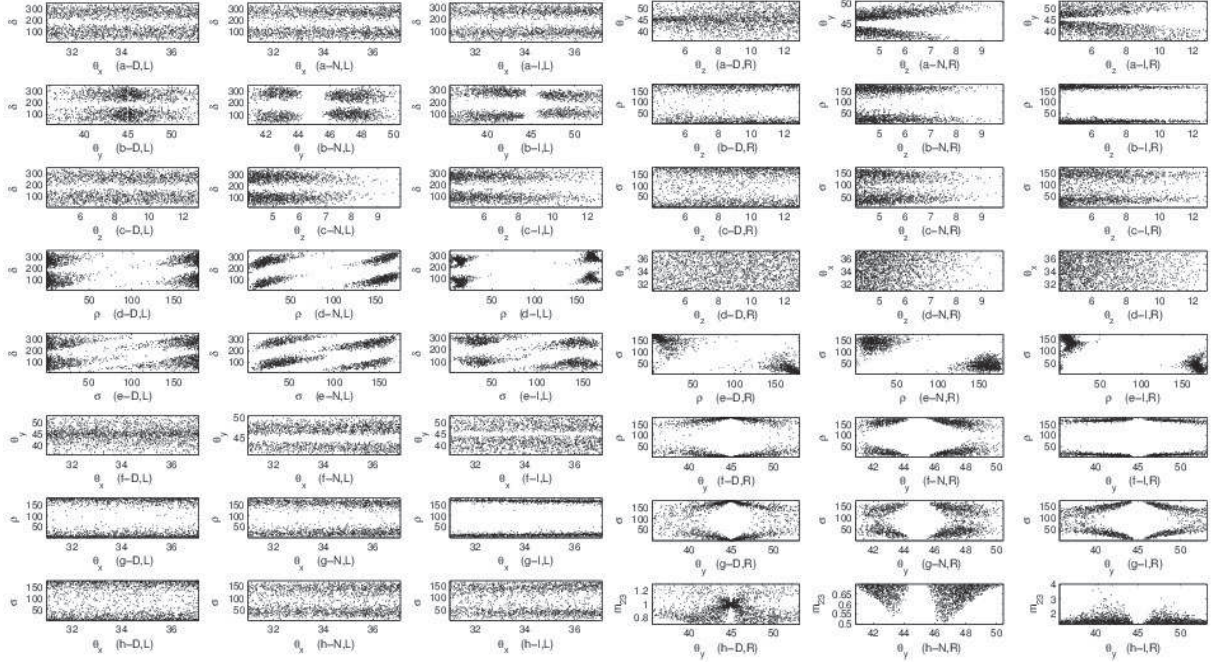


Figure 4: Pattern having $M_{\nu 12} (1 + \chi) + M_{\nu 13} = 0$, and $M_{\nu 22} - M_{\nu 33} = 0$: The left panel (the left three columns) presents correlations of δ against mixing angles and Majorana phases (ρ and σ) and those of θ_x against θ_y , ρ and σ . The right panel (the right three columns) shows the correlations of θ_z against θ_y , ρ , σ , and θ_x and those of ρ against σ and θ_y , and also the correlation of θ_y versus σ and m_{23} .

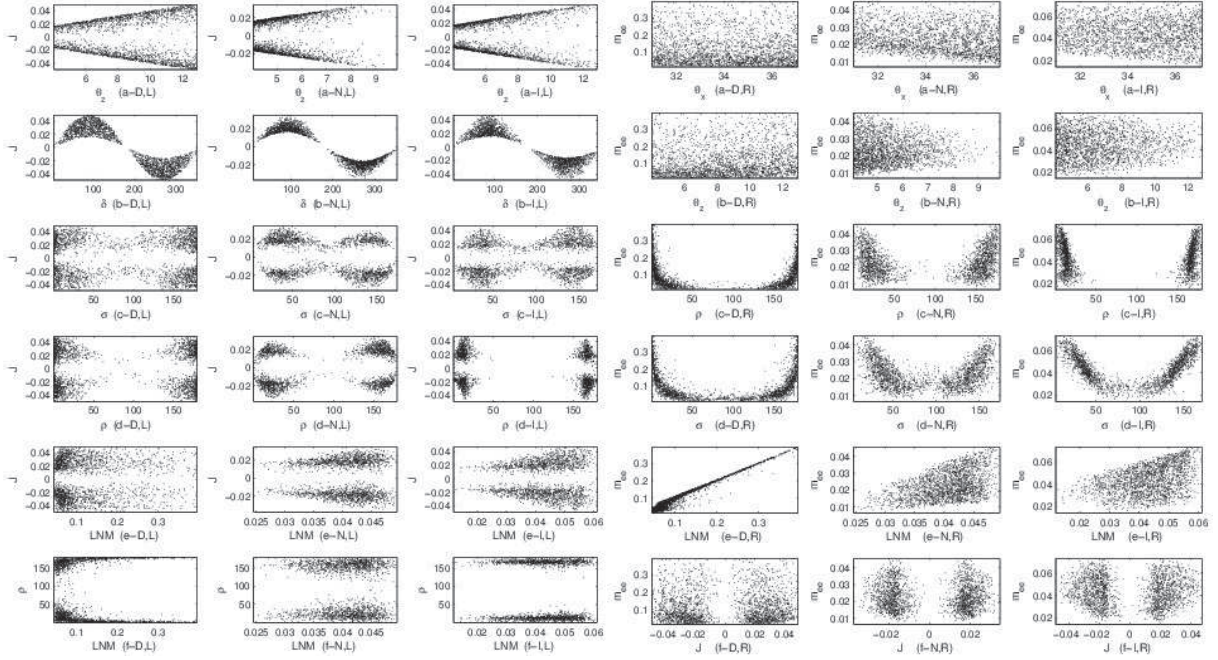


Figure 5: Pattern having $M_{\nu 12} (1 + \chi) + M_{\nu 13} = 0$, and $M_{\nu 22} - M_{\nu 33} = 0$: Left panel presents correlations of J against θ_z , δ , σ , ρ , and lowest neutrino mass (LNM), while the last one depicts the correlation of LNM against ρ . The right panel shows correlations of m_{ee} against θ_x , θ_z , ρ , σ , LNM and J .

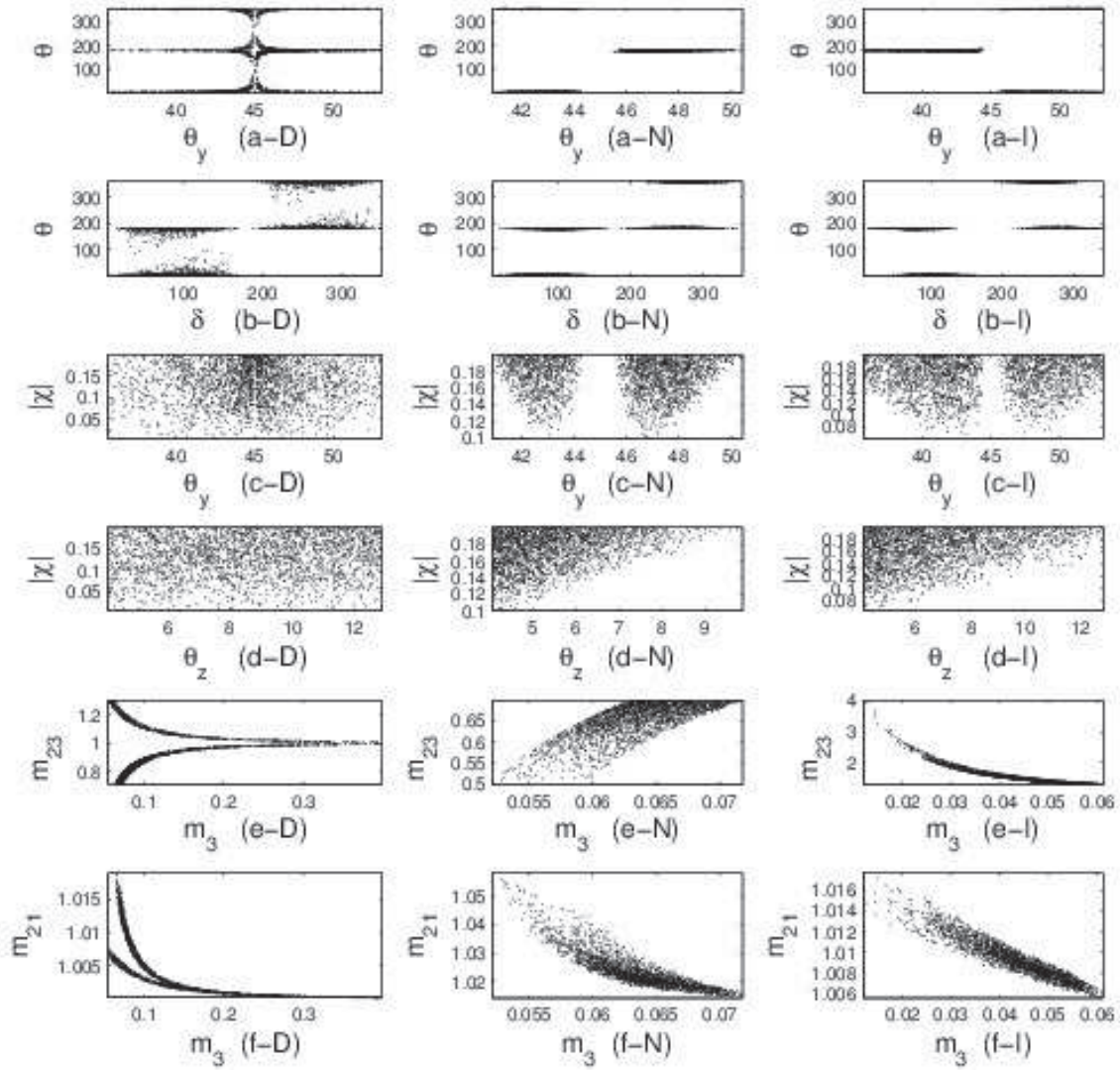


Figure 6: Pattern having $M_{\nu 12} (1 + \chi) + M_{\nu 13} = 0$, and $M_{\nu 22} - M_{\nu 33} = 0$: The first two rows presents the correlations of θ against θ_y and δ , while the second two rows depict those of $|\chi|$ versus θ_y and θ_z . The last two rows shows the correlations of mass ratios m_{23} and m_{21} against m_3 .

7.3 C3: Pattern having $M_{\nu 12} - M_{\nu 13} = 0$, and $M_{\nu 22} (1 + \chi) - M_{\nu 33} = 0$.

In this pattern, the relevant expressions for A 's and B 's are

$$\begin{aligned}
A_1 &= -c_x c_z (c_x s_y s_z + s_x c_y e^{-i\delta}) - c_x c_z (-c_x c_y s_z + s_x s_y e^{-i\delta}), \\
A_2 &= s_x c_z (-s_x s_y s_z + c_x c_y e^{-i\delta}) + s_x c_z (s_x c_y s_z + c_x s_y e^{-i\delta}), \\
A_3 &= s_z c_z (s_y - c_y), \\
B_1 &= (c_x s_y s_z + s_x c_y e^{-i\delta})^2 (1 + \chi) - (-c_x c_y s_z + s_x s_y e^{-i\delta})^2, \\
B_2 &= (-s_x s_y s_z + c_x c_y e^{-i\delta})^2 (1 + \chi) - (s_x c_y s_z + c_x s_y e^{-i\delta})^2, \\
B_3 &= s_y^2 c_z^2 (1 + \chi) - c_y^2 c_z^2,
\end{aligned} \tag{63}$$

leading to mass ratios, up to leading order in s_z , as

$$m_{13} \approx \sqrt{\frac{T_3}{T_4}} \left[1 - \frac{|\chi| c_{2y} (-c_\delta s_y^2 |\chi| + c_{2y} c_{\delta-\theta}) s_z}{t_x (1 + s_{2y}) T_3} \right] + O(s_z^2),$$

$$m_{23} \approx \sqrt{\frac{T_3}{T_4}} \left[1 + \frac{|\chi| c_{2y} t_x (-c_\delta s_y^2 |\chi| + c_{2y} c_{\delta-\theta}) s_z}{(1 + s_{2y}) T_3} \right] + O(s_z^2), \quad (64)$$

where T_3 and T_4 are defined as,

$$\begin{aligned} T_3 &= |\chi|^2 s_y^4 - 2 |\chi| c_\theta s_y^2 c_{2y} + c_{2y}^2, \\ T_4 &= |\chi|^2 c_y^4 + 2 |\chi| c_\theta c_y^2 c_{2y} + c_{2y}^2, \end{aligned} \quad (65)$$

While the Majorana phases as,

$$\begin{aligned} \rho &\approx \frac{1}{2} \arctan \left[\frac{|\chi|^2 c_y^2 s_y^2 s_{2\delta} - |\chi| c_{2y} (2 c_y^2 s_{2\delta} c_\theta - s_{2\delta+\theta}) - s_{2\delta} c_{2y}^2}{|\chi|^2 c_y^2 s_y^2 c_{2\delta} - |\chi| c_{2y} (2 c_y^2 c_{2\delta} c_\theta - c_{2\delta+\theta}) - c_{2\delta} c_{2y}^2} \right] + O(s_z), \\ &\approx \delta \quad \text{for small enough } |\chi|; |\chi| \leq 0.2, \\ \sigma &\approx \frac{1}{2} \arctan \left[\frac{|\chi|^2 c_y^2 s_y^2 s_{2\delta} - |\chi| c_{2y} (2 c_y^2 s_{2\delta} c_\theta - s_{2\delta+\theta}) - s_{2\delta} c_{2y}^2}{|\chi|^2 c_y^2 s_y^2 c_{2\delta} - |\chi| c_{2y} (2 c_y^2 c_{2\delta} c_\theta - c_{2\delta+\theta}) - c_{2\delta} c_{2y}^2} \right] + O(s_z), \\ &\approx \delta \quad \text{for small enough } |\chi|; |\chi| \leq 0.2. \end{aligned} \quad (66)$$

The parameters R_ν , mass ratio square difference $m_{23}^2 - m_{13}^2$, $\langle m \rangle_e$ and $\langle m \rangle_{ee}$ can be deduced to be,

$$\begin{aligned} R_\nu &\approx \frac{2 |\chi| c_{2y} (-c_\delta s_y^2 |\chi| + c_{2y} c_{\delta-\theta}) s_z}{s_x c_x (1 + s_{2y}) T_4} + O(s_z^2), \\ m_{23}^2 - m_{13}^2 &\approx \frac{2 |\chi| c_{2y} (-c_\delta s_y^2 |\chi| + c_{2y} c_{\delta-\theta}) s_z}{s_x c_x (1 + s_{2y}) T_4} + O(s_z^2), \\ \langle m \rangle_e &\approx m_3 \sqrt{\frac{T_3}{T_4}} \left[1 + \frac{2 s_z |\chi| c_{2y} (|\chi| s_y^2 c_\delta - c_{2y} c_{\delta-\theta})}{t_{2x} (1 + s_{2y}) T_3} \right] + O(s_z^2), \\ \langle m \rangle_{ee} &\approx m_3 \sqrt{\frac{T_3}{T_4}} \left[1 + \frac{2 s_z |\chi| c_{2y} (|\chi| s_y^2 c_\delta - c_{2y} c_{\delta-\theta})}{t_{2x} (1 + s_{2y}) T_3} \right] + O(s_z^2). \end{aligned} \quad (67)$$

It is worthy to mention that the expansions in terms of s_z for this pattern are well behaved in the sense that the expansion coefficients appearing in the mass ratio expressions are not divergent for certain values of the mixing angles as it is the case in the C1 and C2 patterns. Therefore, the expansion can be reliably used as a perturbative expansion in which higher order terms have negligible contribution compared to the lower ones. In this pattern, it remains forbidden for θ_z or the difference $(\theta_y - \frac{\pi}{4})$ to vanish otherwise, as exact computations show, we would have degeneracy for m_1 and m_2 leading to vanishing R_ν . In contrast, the phases δ (Dirac phase) and θ can attain the values zero or π without implying vanishing R_ν . These findings can be easily deduced using the approximate formula for R_ν as given in Eq. (67). The complete degeneracy ($m_1 = m_2 = m_3$) is achieved when $\theta_y = \frac{\pi}{4}$ and $\delta = \frac{\pi}{2}$ which can only be checked using the exact complicated formulae for m_{13} and m_{23} . At this particular value, $(\theta_y = \frac{\pi}{4}, \delta = \frac{\pi}{2})$, the zeroth order expansion coefficient, of say $m_{13}\sqrt{T_4/T_3}$, assumes the value of one, while the other remaining coefficients are checked to be vanishing. The positivity of R_ν and the constraint to lie within the interval $[0.0262, 0.0397]$ (at $3 - \sigma$ level) imposes a complicated relation between δ and θ rather than the simple constraint of belonging to alternate (identical) semicircles in the cases C1 (C2).

The phenomenology of this pattern has many features in common with that of the pattern C1 in terms of correlations and allowed values for the parameters as can be checked from the corresponding Figs.-(7-9) versus (1-3)- and Tables (3-4). Thus, we shall not repeat the same discussions and descriptions. Rather, we mention few dissimilarities: first, the mixing angle θ_y is allowed to cover all of its admissible range even in the cases of inverted and normal hierarchies; second, the correlation between δ and θ is not as simple as that of belonging to opposite semicircles in the pattern C1, where the R_ν 's expression allows interpreting it.

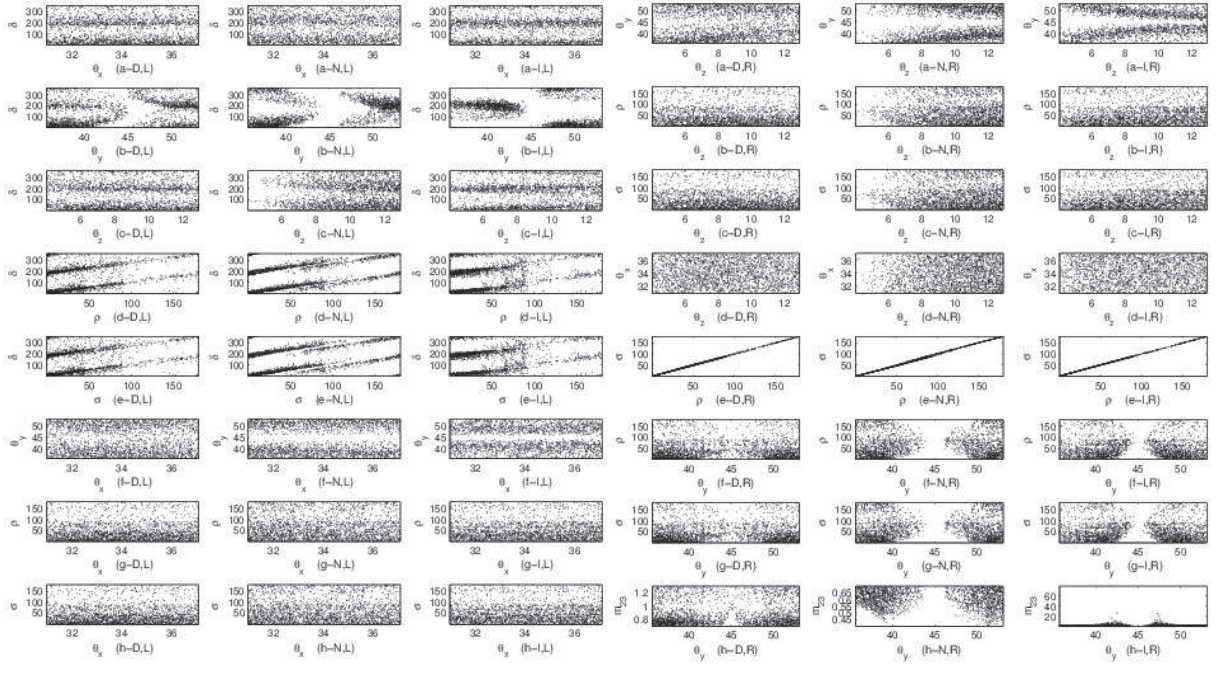


Figure 7: Pattern having $M_{\nu 12} - M_{\nu 13} = 0$, and $M_{\nu 22} (1 + \chi) - M_{\nu 33} = 0$: The left panel (the left three columns) presents correlations of δ against mixing angles and Majorana phases (ρ and σ) and those of θ_x against θ_y , ρ and σ . The right panel (the right three columns) shows the correlations of θ_z against θ_y , ρ , σ , and θ_x and those of ρ against σ and θ_y , and also the correlation of θ_y versus σ and m_{23} .

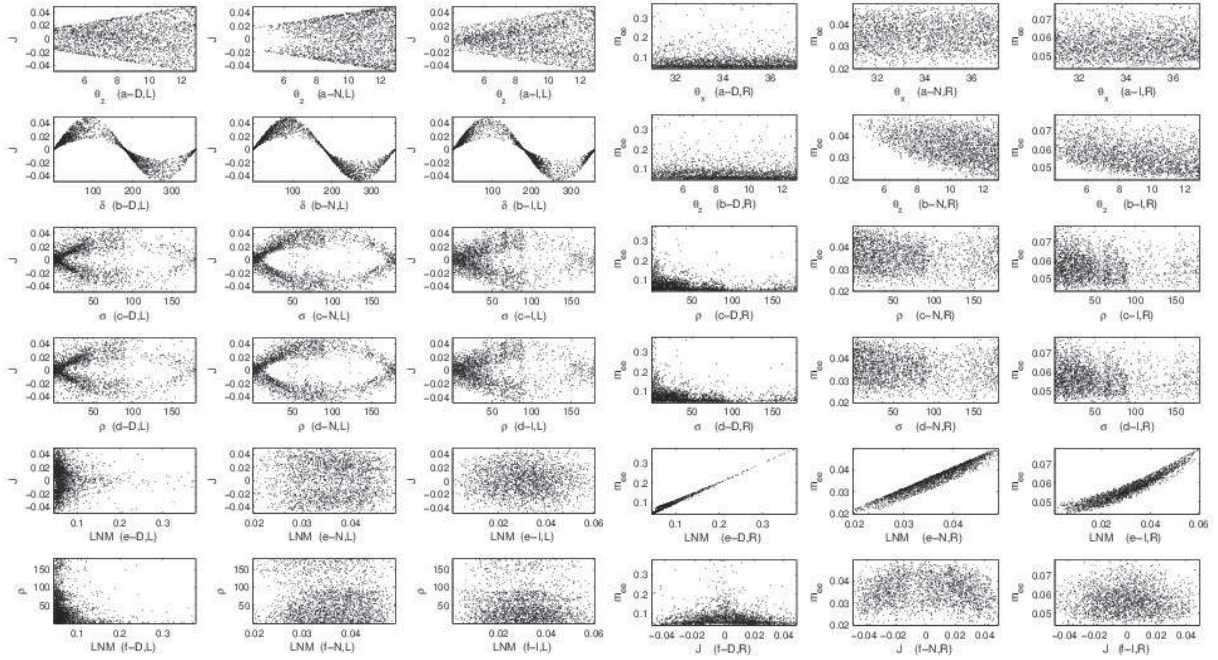


Figure 8: Pattern having $M_{\nu 12} - M_{\nu 13} = 0$, and $M_{\nu 22} (1 + \chi) - M_{\nu 33} = 0$: Left panel presents correlations of J against θ_z , δ , σ , ρ , and lowest neutrino mass (LNM), while the last one depicts the correlation of LNM against ρ . The right panel shows correlations of m_{ee} against θ_x , θ_z , ρ , σ , LNM and J .

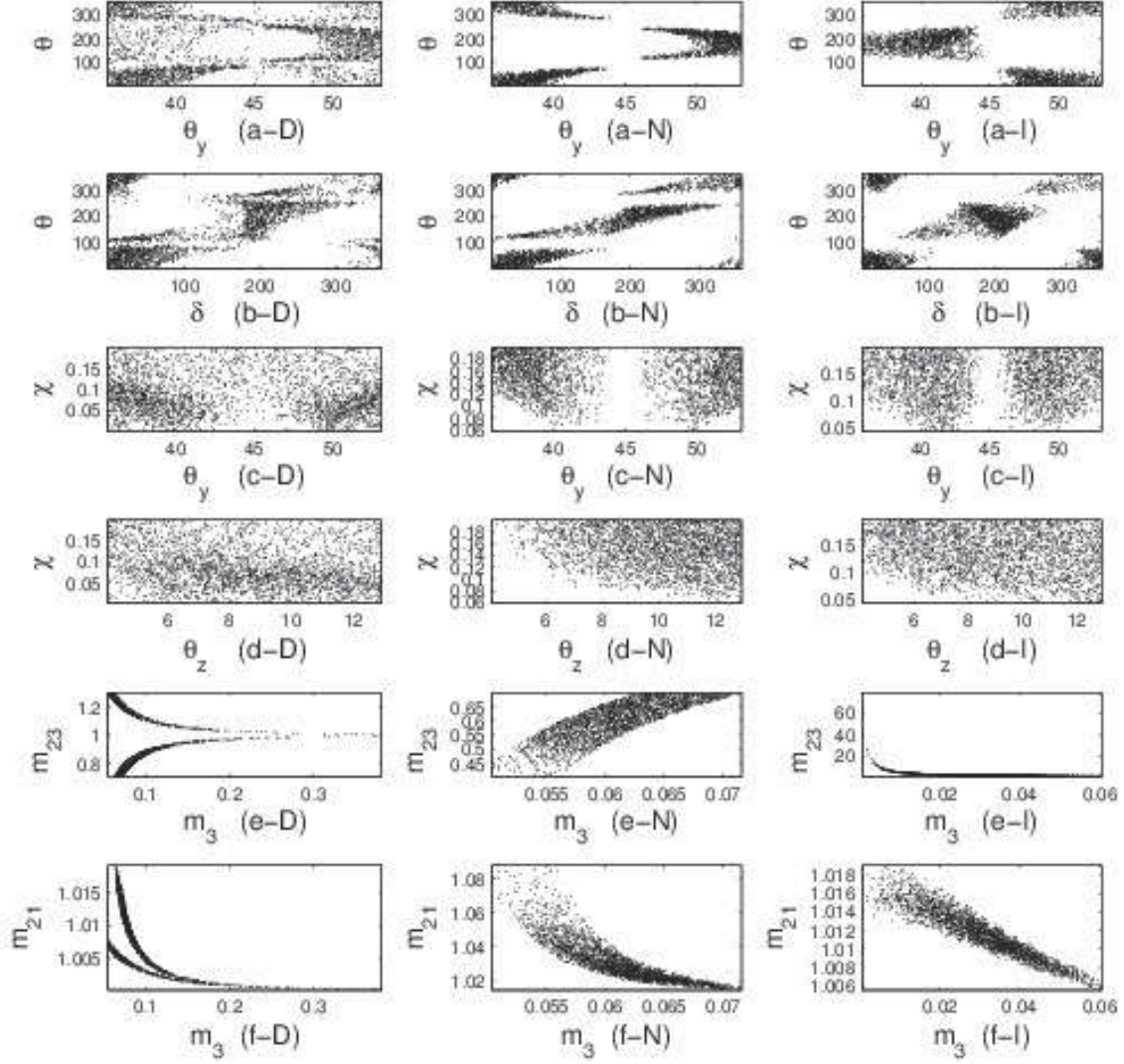


Figure 9: Pattern having $M_{\nu 12} - M_{\nu 13} = 0$, and $M_{\nu 22} (1 + \chi) - M_{\nu 33} = 0$: The first two rows presents the correlations of θ against θ_y and δ , while the second two rows depict those of $|\chi|$ versus θ_y and θ_z . The last two rows shows the correlations of mass ratios m_{23} and m_{21} against m_3 .

7.4 C4: Pattern having $M_{\nu 12} + M_{\nu 13} = 0$, and $M_{\nu 22} (1 + \chi) - M_{\nu 33} = 0$.

In this pattern, the relevant expressions for A 's and B 's are

$$\begin{aligned}
A_1 &= -c_x c_z (c_x s_y s_z + s_x c_y e^{-i\delta}) + c_x c_z (-c_x c_y s_z + s_x s_y e^{-i\delta}), \\
A_2 &= s_x c_z (-s_x s_y s_z + c_x c_y e^{-i\delta}) - s_x c_z (s_x c_y s_z + c_x s_y e^{-i\delta}), \\
A_3 &= s_z c_z (s_y + c_y), \\
B_1 &= (c_x s_y s_z + s_x c_y e^{-i\delta})^2 (1 + \chi) - (-c_x c_y s_z + s_x s_y e^{-i\delta})^2, \\
B_2 &= (-s_x s_y s_z + c_x c_y e^{-i\delta})^2 (1 + \chi) - (s_x c_y s_z + c_x s_y e^{-i\delta})^2, \\
B_3 &= s_y^2 c_z^2 (1 + \chi) - c_y^2 c_z^2,
\end{aligned} \tag{68}$$

leading to mass ratios, up to leading order in s_z , as

$$m_{13} \approx \sqrt{\frac{T_3}{T_4}} \left[1 + \frac{|\chi| c_{2y} (-c_\delta s_y^2 |\chi| + c_{2y} c_{\delta-\theta}) s_z}{t_x (1 - s_{2y}) T_3} \right] + O(s_z^2),$$

$$m_{23} \approx \sqrt{\frac{T_3}{T_4}} \left[1 - \frac{|\chi| c_{2y} t_x (-c_\delta s_y^2 |\chi| + c_{2y} c_{\delta-\theta}) s_z}{(1-s_{2y}) T_3} \right] + O(s_z^2). \quad (69)$$

While the Majorana phases as,

$$\begin{aligned} \rho &\approx \frac{1}{2} \arctan \left[\frac{|\chi|^2 c_y^2 s_y^2 s_{2\delta} - |\chi| c_{2y} (2c_y^2 s_{2\delta} c_\theta - s_{2\delta+\theta}) - s_{2\delta} c_{2y}^2}{|\chi|^2 c_y^2 s_y^2 c_{2\delta} - |\chi| c_{2y} (2c_y^2 c_{2\delta} c_\theta - c_{2\delta+\theta}) - c_{2\delta} c_{2y}^2} \right] + O(s_z), \\ \sigma &\approx \frac{1}{2} \arctan \left[\frac{|\chi|^2 c_y^2 s_y^2 s_{2\delta} - |\chi| c_{2y} (2c_y^2 s_{2\delta} c_\theta - s_{2\delta+\theta}) - s_{2\delta} c_{2y}^2}{|\chi|^2 c_y^2 s_y^2 c_{2\delta} - |\chi| c_{2y} (2c_y^2 c_{2\delta} c_\theta - c_{2\delta+\theta}) - c_{2\delta} c_{2y}^2} \right] + O(s_z). \end{aligned} \quad (70)$$

The parameters R_ν , mass ratio square difference $m_{23}^2 - m_{13}^2$, $\langle m \rangle_e$ and $\langle m \rangle_{ee}$ can be deduced to be,

$$\begin{aligned} R_\nu &\approx \frac{2 |\chi| c_{2y} (+c_\delta s_y^2 |\chi| - c_{2y} c_{\delta-\theta}) s_z}{s_x c_x (1-s_{2y}) T_4} + O(s_z^2), \\ m_{23}^2 - m_{13}^2 &\approx \frac{2 |\chi| c_{2y} (+c_\delta s_y^2 |\chi| - c_{2y} c_{\delta-\theta}) s_z}{s_x c_x (1-s_{2y}) T_4} + O(s_z^2), \\ \langle m \rangle_e &\approx m_3 \sqrt{\frac{T_3}{T_4}} \left[1 - \frac{2 s_z |\chi| c_{2y} (|\chi| s_y^2 c_\delta - c_{2y} c_{\delta-\theta})}{t_{2x} (1-s_{2y}) T_3} \right] + O(s_z^2), \\ \langle m \rangle_{ee} &\approx m_3 \sqrt{\frac{T_3}{T_4}} \left[1 - \frac{2 s_z |\chi| c_{2y} (|\chi| s_y^2 c_\delta - c_{2y} c_{\delta-\theta})}{t_{2x} (1-s_{2y}) T_3} \right] + O(s_z^2). \end{aligned} \quad (71)$$

Once again, and as it was for the two patterns C1 and C2, one can find the same interrelations between C3 and C4 where the results (formulae) of C4 can be derived from those of C3, by simply making the substitutions $s_y \rightarrow -s_y$ and $\delta \rightarrow \delta + \pi$. Another time, the found relations cannot be used in a useful way to derive the predictions of one pattern from the other because the mapping $s_y \rightarrow -s_y$ does not keep the physically admissible region of θ_y invariant. Furthermore, we are ill-fated that the properties regarding boundedness of the expansion coefficients of the mass ratios are mapped so that the bounded coefficient at $(\theta_y = \frac{\pi}{4}, \delta = \frac{\pi}{2})$ in the pattern C3 may become divergent in the case of C4. This becomes clear by looking at the expressions in Eq. (69), where the zeroth order expansion coefficient, for say $m_{13} \sqrt{T_4/T_3}$, assumes the value one, and the first order coefficient is convergent at $(\theta_y = \frac{\pi}{4}, \delta = \frac{\pi}{2})$, whereas all higher order expansion coefficients are divergent at this point while they were vanishing in the C3 pattern. This finding is consistent with the infinite number of divergent terms summing up to a smooth function as was discussed in Section (7.1). The divergence for R_ν expansion is starting from the second order coefficient in harmony with the corresponding behaviour in the patterns C1 and C2. Using the exact expression of R_ν corresponding to this pattern shows that the mixing angle θ_y is allowed to be exactly $\frac{\pi}{4}$ without forcing R_ν to vanish. The phases δ and θ can assume also any arbitrary values, but we should note that the point $(\theta_y = \frac{\pi}{4}, \delta = \frac{\pi}{2})$ causes the exact form of R_ν to be null. It is obvious that vanishing θ_z leads also to vanishing R_ν , but this choice is already excluded by data. As was the case in the C3 pattern, the correlation between δ and θ that emerges from the positivity of R_ν and its allowed range cannot, due to the complicated expression of R_ν that involves complicated dependence on phases even at the approximate level, be described in a simple manner. We stress again that the expansion should be dealt and interpreted with caution in case of divergent coefficients and cannot be reliably used as perturbative expansion. Thus to avoid these kinds of problems, our numerical results are based on exact expressions that do not suffer from divergences.

We checked when we spanned the parameter space that the normal hierarchy could accommodate the data only at the $3 - \sigma$ error level, whereas the inverted hierarchy could do it at the $2 - 3 \sigma$ error levels, and the degenerate hierarchy could survive at all error levels. The figures (10, 11 and 12) show the corresponding correlation plots, with the same conventions as in the previous patterns. The appearance of the normal hierarchy only at the $3 - \sigma$ error level makes it so special, and it turns out to be quite restrictive in the sense that the mixing angle θ_y is severely bounded to be around two possible values, namely, 36° or 52° , whereas θ_z has only one narrow band close to 4° , while the Dirac phase δ covers almost all its range excluding the region $]158^\circ - 188.4^\circ[$. Moreover, in this normal hierarchy case the

parameter χ , parameterizing the deviation from exact μ - τ symmetry, cannot assume an arbitrary value in its prescribed range: $|\chi|$ must be in the range $[0.16 - 0.2]$, whereas the phase θ can cover all its allowable range excluding the region $]19.47^0 - 139.9^0[\cup]217.4^0 - 340.8^0[$.

Once again, there is a close resemblance between the pattern C4 and C2 in terms of correlations and allowed values for the parameters, as can be checked respectively from the corresponding Figs.-(10–12) versus (4–6)- and Tables (3–4). Therefore it is not necessary to repeat the same discussions and descriptions but rather we focus on the few dissimilarities: First, the mixing angle θ_y is allowed to cover all of its admissible range in the inverted hierarchy type, and in particular the value $\frac{\pi}{4}$ which is excluded with its small neighborhood in the pattern C2; second, the Dirac phase δ is allowed to cover all of its ranges in the inverted and degenerate hierarchy types without any exclusion as was the case in the pattern C2 concerning the values (0, and π) together with their neighborhoods; third, the mixing angle θ_z tends to have a far more restrictive range in case of the pattern C4 compared to that of C2; fourth, the normal hierarchy case for the pattern C4, as explained above, represents an exceptional situation, which was not the case in the pattern C2. The figures depicting the correlations for the two patterns C2 and C4 look, more or less, similar provided the loose restrictions on θ_y and δ associated with the pattern C4 are taken into consideration.

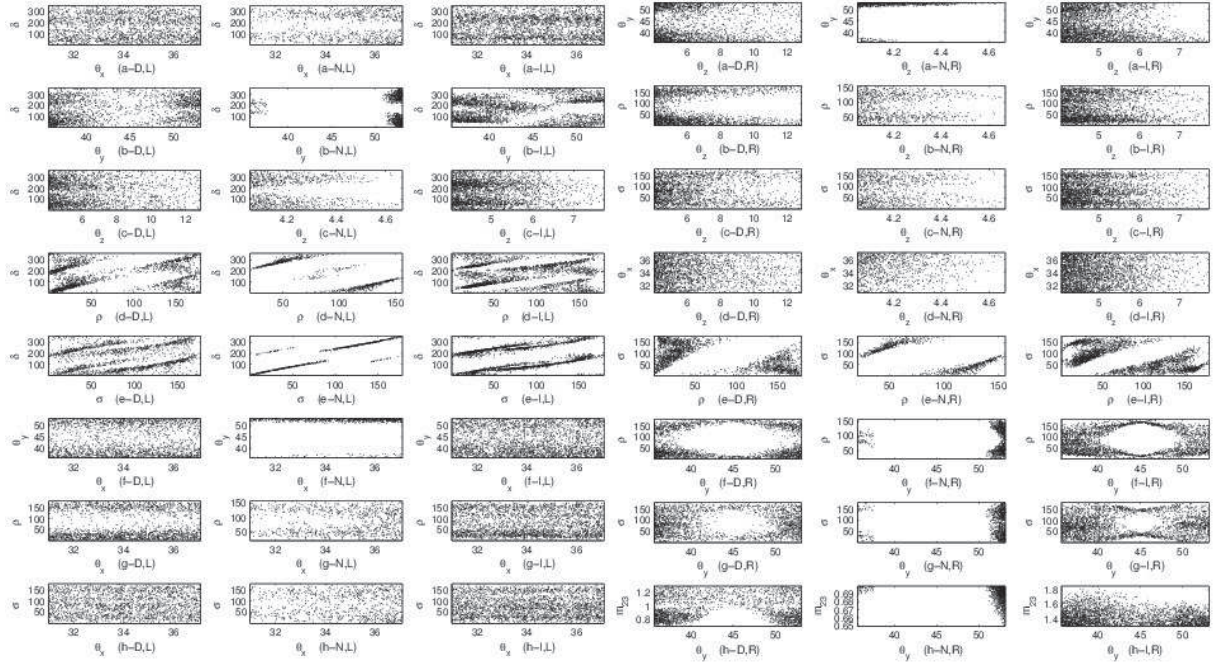


Figure 10: Pattern having $M_{\nu 12} + M_{\nu 13} = 0$, and $M_{\nu 22} (1 + \chi) - M_{\nu 33} = 0$: The left panel (the left three columns) presents correlations of δ against mixing angles and Majorana phases (ρ and σ) and those of θ_x against θ_y , ρ and σ . The right panel (the right three columns) shows the correlations of θ_z against θ_y , ρ , σ , and θ_x and those of ρ against σ and θ_y , and also the correlation of θ_y versus σ and m_{23} .

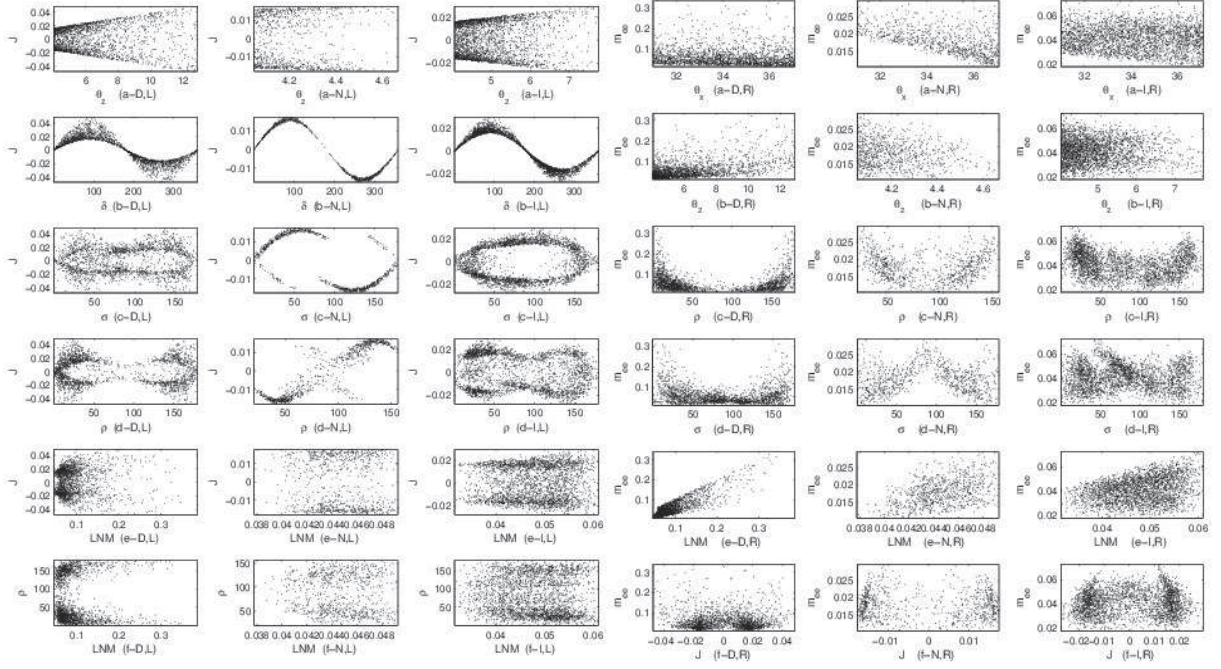


Figure 11: Pattern having $M_{\nu 12} + M_{\nu 13} = 0$, and $M_{\nu 22}(1 + \chi) - M_{\nu 33} = 0$: Left panel presents correlations of J against θ_z , δ , σ , ρ , and lowest neutrino mass (**LNM**), while the last one depicts the correlation of LNM against ρ . The right panel shows correlations of m_{ee} against θ_x , θ_z , ρ , σ , **LNM** and J .

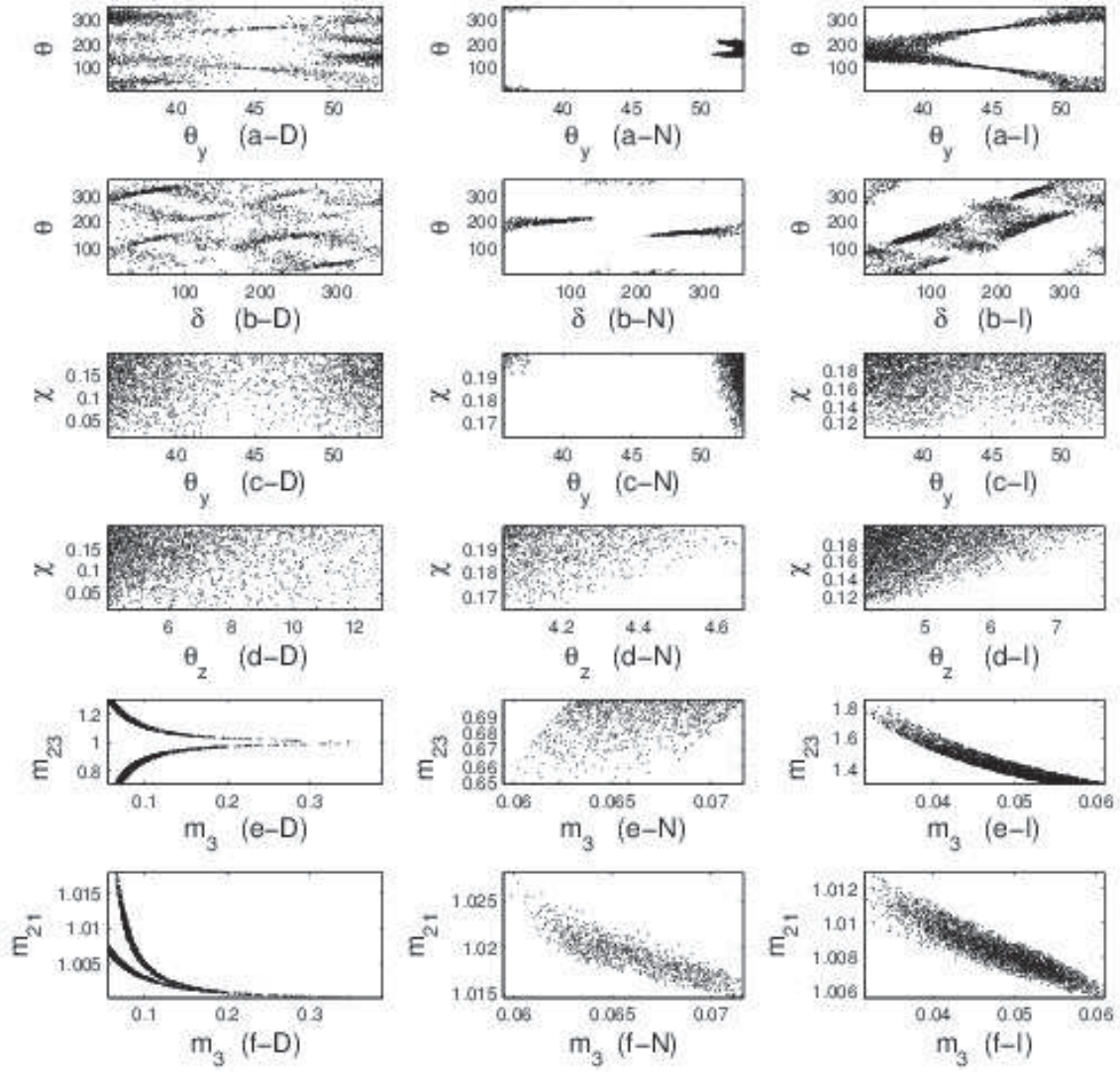


Figure 12: Pattern having $M_{\nu 12} + M_{\nu 13} = 0$, and $M_{\nu 22}(1 + \chi) - M_{\nu 33} = 0$: The first two rows presents the correlations of θ against θ_y and δ , while the second two rows depict those of $|\chi|$ versus θ_y and θ_z . The last two rows shows the correlations of mass ratios m_{23} and m_{21} against m_3 .

Pattern: $M_{\nu 12}(1+\chi) - M_{\nu 13} = 0$, and $M_{\nu 22} - M_{\nu 33} = 0$												
quantity	θ_x	θ_y	θ_z	m_1	m_2	m_3	ρ	σ	δ	$(m)_e$	$(m)_{ee}$	J
1 σ	32.96 – 35.00	38.77 – 44.99	7.71 – 10.30	0.0470 – 0.3975	0.0478 – 0.3976	0.0583 – 0.3971	0.1010 – 177.00	0.1915 – 176.96	[0.3653 – 176.6] [180.8 – 358.27]	0.0479 – 0.3975	0.0448 – 0.3939	–0.0402 – 0.0402
2 σ	31.95 – 36.09	36.88 – 50.77	6.29 – 11.68	0.0463 – 0.3942	0.0471 – 0.3943	0.0568 – 0.3970	0.2341 – 178.17	0.2670 – 178.16	[0.7333 – 173.3] [180.3 – 357.99]	0.0470 – 0.3942	0.0429 – 0.3938	–0.0459 – 0.0444
3 σ	30.98 – 37.11	36.96 – 52.01	4.08 – 12.92	0.0457 – 0.3947	0.0465 – 0.3948	0.0557 – 0.3975	0.1981 – 179.55	0.2046 – 179.46	[0.1882 – 176.7] [180.6 – 359.79]	0.0463 – 0.3949	0.0411 – 0.3947	–0.0502 – 0.0506
Normal Hierarchy												
1 σ	32.96 – 35.00	44.29 – 44.96	7.71 – 10.30	0.0163 – 0.0471	0.0186 – 0.0479	0.0510 – 0.0686	9.71 – 167.30	9.77 – 167.1	[14.44 – 167.1] [188 – 354.00]	0.019 – 0.0481	0.0151 – 0.0476	[–0.0406 – –0.0041] [0.0079 – 0.0404]
2 σ	31.95 – 36.09	[44.03 – 44.95] [45.05 – 46.07]	6.29 – 11.68	0.0129 – 0.0483	0.0149 – 0.0491	0.0497 – 0.0703	7.36 – 171.71	7.32 – 171.56	[3.22 – 166.9] [188.2 – 346.46]	0.0166 – 0.0496	0.0115 – 0.0485	[–0.0456 – –0.0061] [0.0021 – 0.0457]
3 σ	30.98 – 37.10	[43.87 – 44.98] [45.04 – 46.30]	4.11 – 12.92	0.0124 – 0.0490	0.0151 – 0.0498	0.0485 – 0.0714	4.48 – 175.92	4.88 – 175.83	[8.71 – 173.5] [190.1 – 357.69]	0.0168 – 0.050	0.0107 – 0.0496	[–0.0504 – –0.0019] [0.0053 – 0.050]
Inverted Hierarchy												
1 σ	32.96 – 35.00	43.89 – 44.97	7.71 – 10.30	0.0463 – 0.0783	0.0471 – 0.0787	7.4×10^{-4} – 0.0602	0.2721 – 179.84	0.0356 – 179.49	[2.87 – 117.4] [235.6 – 357.6]	0.0459 – 0.0779	0.0452 – 0.0779	[–0.0403 – –0.0017] [0.0020 – 0.0402]
2 σ	31.95 – 36.08	[43.57 – 44.97] [45.04 – 46.13]	6.29 – 11.68	0.0460 – 0.0783	0.0474 – 0.0788	8.48×10^{-4} – 0.0601	0.0617 – 179.40	0.0771 – 179.81	[7.11 – 174.1] [185.7 – 356.34]	0.0461 – 0.0780	0.0453 – 0.0775	[–0.0453 – –0.0020] [0.0033 – 0.0456]
3 σ	30.98 – 37.11	[43.46 – 44.98] [45.02 – 46.35]	4.05 – 12.92	0.0452 – 0.0802	0.0460 – 0.0806	3.2×10^{-4} – 0.0617	0.8583 – 179.39	0.5892 – 179.73	[6.60 – 172.4] [188.7 – 352.83]	0.0445 – 0.0796	0.0436 – 0.0784	[–0.0501 – –0.0036] [0.0036 – 0.0504]
Pattern: $M_{\nu 12}(1+\chi) - M_{\nu 13} = 0$, and $M_{\nu 22} - M_{\nu 33} = 0$												
quantity	θ_x	θ_y	θ_z	m_1	m_2	m_3	ρ	σ	δ	$(m)_e$	$(m)_{ee}$	J
Degenerate Hierarchy												
1 σ	32.96 – 35.00	38.65 – 45.91	7.71 – 10.30	0.0475 – 0.3950	0.0483 – 0.3951	0.0579 – 0.3970	[0.1509 – 40.42] [136.9 – 179.95]	0.3750 – 179.29	[2.83 – 164.7] [199.5 – 356.94]	0.0482 – 0.3950	0.0193 – 0.3947	–0.0396 – 0.0406
2 σ	31.95 – 36.10	36.87 – 50.77	6.29 – 11.68	0.0471 – 0.3959	0.0479 – 0.3960	0.0579 – 0.3927	[0.0045 – 88.53] [111.5 – 179.95]	0.5585 – 179.45	[1.96 – 174.7] [189.9 – 352.1]	0.0477 – 0.3958	0.0155 – 0.3958	[–0.0453 – –0.004] [0.001 – 0.0448]
3 σ	30.98 – 37.11	35.67 – 53.10	4.05 – 12.92	0.0454 – 0.3947	0.0462 – 0.3948	0.0554 – 0.3980	[0.0064 – 93.2] [109.53 – 179.90]	0.6741 – 179.36	[4.71 – 167.8] [188 – 350.9698]	0.0459 – 0.3949	0.0148 – 0.3941	[–0.0496 – –0.0034] [0.0019 – 0.0492]
Normal Hierarchy												
1 σ	32.98 – 34.99	40.85 – 42.05	7.71 – 8.16	0.0444 – 0.0474	0.0452 – 0.0482	0.0655 – 0.0689	[5.01 – 23.17] [156.9 – 177.81]	[41.78 – 74.46] [100.3 – 137.8190]	[15.28 – 78.84] [279 – 352.81]	0.0451 – 0.0481	0.0175 – 0.0298	[–0.0304 – –0.0123] [0.008 – 0.0302]
2 σ	31.95 – 36.09	[40.70 – 43.12] [46.45 – 50.31]	6.29 – 9.89	0.0345 – 0.0485	0.0356 – 0.0493	0.0586 – 0.0704	[0.1354 – 59.76] [121.2 – 179.89]	18.58 – 162.63	[12.42 – 177.6] [185.9 – 345.12]	0.0353 – 0.0493	0.0120 – 0.0406	[–0.0346 – –0.003] [0.005 – 0.0371]
3 σ	30.98 – 37.11	[40.88 – 44.26] [45.52 – 50.43]	4.05 – 9.87	0.0246 – 0.0495	0.0260 – 0.0502	0.0521 – 0.0718	[0.0144 – 89.4] [112.4 – 179.44]	4.49 – 173.68	[10.79 – 167.3] [187.6 – 353.32]	0.0253 – 0.0500	0.0067 – 0.0453	[–0.0374 – –0.0024] [0.0045 – 0.0347]
Inverted Hierarchy												
1 σ	32.96 – 35.00	38.65 – 43.46	7.71 – 10.30	0.0551 – 0.0784	0.0558 – 0.0789	0.0294 – 0.0603	[3.54 – 19.71] [160.2 – 176.77]	[14.78 – 69.1] [109.7165.11]	[18.51 – 121.2] [236.7 – 343.59]	0.0550 – 0.0781	0.0289 – 0.0717	[–0.0400 – –0.01] [0.01 – 0.0398]
2 σ	31.95 – 36.09	[36.89 – 43.81] [46.3 – 50.77]	6.29 – 11.67	0.0526 – 0.0784	0.0534 – 0.0788	0.0248 – 0.0602	[0.4268 – 28.53] [153.5 – 177.64]	9.58 – 168.19	[6.25 – 157.6] [196.6 – 347.4449]	0.0526 – 0.0779	0.0199 – 0.0724	[–0.0439 – –0.007] [0.003 – 0.0438]
3 σ	30.98 – 37.11	[35.7 – 44.39] [45.57 – 53.13]	4.05 – 12.84	0.0468 – 0.0797	0.0476 – 0.0802	0.0118 – 0.0612	[0.1457 – 48.96] [137.7 – 179.93]	4.47 – 170.68	[4.56 – 162.9] [190.2 – 341.24]	0.0469 – 0.0798	0.0145 – 0.0730	[–0.0488 – –0.0038] [0.0019 – 0.0470]
Pattern: $M_{\nu 12} - M_{\nu 13} = 0$, and $M_{\nu 22}(1+\chi) - M_{\nu 33} = 0$												
quantity	θ_x	θ_y	θ_z	m_1	m_2	m_3	ρ	σ	δ	$(m)_e$	$(m)_{ee}$	J
Degenerate Hierarchy												
1 σ	32.96 – 35	38.65 – 44.848	7.71 – 10.30	0.0472 – 0.3790	0.0480 – 0.3791	0.0579 – 0.3822	0.0149 – 179.30	0.0169 – 179.29	0.0484 – 359.94	0.0480 – 0.3791	0.0447 – 0.3718	–0.0398 – 0.0398
2 σ	31.95 – 36.09	[36.87 – 44.88] [45.13 – 50.77]	6.29 – 11.68	0.0465 – 0.3951	0.0473 – 0.3952	0.0574 – 0.3921	0.0305 – 179.84	0.0546 – 179.84	0.0702 – 359.88	0.0472 – 0.3950	0.0435 – 0.3949	–0.0442 – 0.0447
3 σ	30.98 – 37.11	[35.67 – 44.93] [45.08 – 53.1295]	4.06 – 12.92	0.0453 – 0.3777	0.0462 – 0.3778	0.0556 – 0.3810	0.0191 – 180	0.0192 – 180	0.0257 – 359.86	0.0463 – 0.3779	0.0421 – 0.3761	–0.0488 – 0.0487
Normal Hierarchy												
1 σ	32.96 – 35	38.65 – 43.72	7.72 – 10.30	0.0259 – 0.0473	0.0272 – 0.0481	0.0550 – 0.0689	0.2150 – 179.98	0.0609 – 179.97	[0.1287 – 172.7] [193.3 – 359.1856]	0.0277 – 0.0481	0.0256 – 0.0479	–0.0393 – 0.0399
2 σ	31.95 – 36.09	[36.88 – 44.04] [46.1 – 50.77]	6.30 – 11.68	0.0223 – 0.0481	0.0239 – 0.0489	0.0531 – 0.0701	0.0070 – 179.98	0.0522 – 179.95	[0.0141 – 171.5] [181.7 – 359.94]	0.0247 – 0.0493	0.0216 – 0.0490	–0.0452 – 0.0456
3 σ	30.98 – 37.11	[35.67 – 43.87] [46.17 – 53.12]	4.08 – 12.92	0.0198 – 0.0492	0.0216 – 0.0500	0.0503 – 0.0715	0.0615 – 180	0.0269 – 179.99	0.1590 – 359.92	0.0228 – 0.0503	0.0199 – 0.0498	–0.0493 – 0.0492
Inverted Hierarchy												
1 σ	32.96 – 35.00	38.65 – 44.36	7.71 – 10.30	0.0464 – 0.0776	0.0472 – 0.0781	0.0008 – 0.0592	0.0224 – 179.77	0.0452 – 179.73	59.89 – 281.52	0.0461 – 0.0774	0.0455 – 0.0773	–0.0390 – 0.0396
2 σ	31.95 – 36.09	[36.89 – 44.32] [45.64 – 50.77]	6.30 – 11.68	0.0463 – 0.0777	0.0471 – 0.0782	0.0019 – 0.0598	0.1213 – 179.93	0.0469 – 179.96	0.1177 – 359.95	0.0458 – 0.0776	0.0448 – 0.0775	–0.0439 – 0.0445
3 σ	30.98 – 37.10	[35.70 – 44.48] [45.63 – 53.13]	4.05 – 12.92	0.0453 – 0.0790	0.0462 – 0.0794	0.0006 – 0.0604	0.0132 – 179.99	0.0244 – 179.84	0.0079 – 359.91	0.0448 – 0.0788	0.0436 – 0.0782	–0.0486 – 0.0492
Pattern: $M_{\nu 12} + M_{\nu 13} = 0$, and $M_{\nu 22}(1+\chi) - M_{\nu 33} = 0$												
quantity	θ_x	θ_y	θ_z	m_1	m_2	m_3	ρ	σ	δ	$(m)_e$	$(m)_{ee}$	J
Degenerate Hierarchy												
1 σ	32.96 – 35	38.65 – 44.98	7.71 – 10.30	0.0757 – 0.3966	0.0755 – 0.3965	0.0293 – 0.3962	[0.0844 – 40.68] [135.6 – 179.67]	1.29 – 177.65	0.2316 – 359.73	0.0745 – 0.3954	0.0483 – 0.3617	–0.0397 – 0.0395
2 σ	31.95 – 36.09	36.87 – 50.77	6.29 – 11.68	0.0658 – 0.3955	0.0664 – 0.3956	0.0374 – 0.3926	[0.0111 – 63.82] [113 – 179.59]	1.38 – 176.99	0.4530 – 359.73	0.0663 – 0.3955	0.0231 – 0.3628	–0.0446 – 0.0443
3 σ	30.99 – 37.10	35.67 – 53.13	4.05 – 12.90	0.0456 – 0.3902	0.0464 – 0.3903	0.0561 – 0.3875	0.1229 – 179.71	0.1735 – 177.30	0.4436 – 359.90	0.0460 – 0.3902	0.0138 – 0.3377	–0.0474 – 0.0484
Normal Hierarchy												
1 σ	x	x	x	x	x	x	x	x	x	x	x	x
2 σ	x	x	x	x	x	x	x	x	x	x	x	x
3 σ	30.99 – 37.11	[35.68 – 37.61] [50.89 – 53.13]	4.05 – 4.67	0.0378 – 0.0493	0.0388 – 0.0501	0.0595 – 0.0717	20.85 – 156.33	0.3957 – 178.58	[0.7022 – 158] [188.4 – 358.43]	0.0383 – 0.0497	0.0104 – 0.0297	–0.0179 – 0.0176
Inverted Hierarchy												
1 σ	x	x	x	x	x	x	x	x	x	x	x	x
2 σ	31.95 – 36.09	36.87 – 50.77	6.29 – 8.07	0.0652 – 0.0787	0.0657 – 0.0792	0.0458 – 0.0605	[0.1822 – 90.22] [94.89 – 178.27]	0.0532 – 179.63	0.1149 – 354.39	0.0651 – 0.0787	0.0203 – 0.0635	–0.0291 – 0.0295
3 σ	30.98 – 37.11	35.68 – 53.12	4.05 – 7.73	0.0554 – 0.0795	0.0561 – 0.0800	0.0314 – 0.0611	0.1136 – 179.52	0.0084 – 179.96	0.2029 – 359.92	0.0555 – 0.0796	0.0175 – 0.0725	–0.0274 – 0.0295

Table 3: The various prediction for the patterns of violating exact μ - τ symmetry. All the angles (masses) are evaluated in degrees (eV).

Pattern: $M_{\nu 12} (1 + \chi) - M_{\nu 13} = 0$, and $M_{\nu 22} - M_{\nu 33} = 0$					
$ \chi $			θ		
1σ	2σ	3σ	1σ	2σ	3σ
Degenerate Hierarchy					
$0.0023 - 0.2$	$0.0030 - 0.2$	$0.0047 - 0.2$	$0.85 - 359.6$	$0.75 - 359.12$	$0.82 - 359.2$
Normal Hierarchy					
$0.0398 - 0.2$	$0.0434 - 0.2$	$0.0378 - 0.2$	$[3.43 - 91] \cup [269.9 - 351.77]$	$[11.74 - 90.57] \cup [101 - 172.5] \cup [188.4 - 263.4] \cup [277.5 - 358.13]$	$[8.73 - 89.7] \cup [104 - 176] \cup [186 - 262] \cup [273.5 - 352.6]$
Inverted Hierarchy					
$0.0309 - 0.2$	$0.020 - 0.2$	$0.0276 - 0.2$	$[13.51 - 1272.2] \cup [188.1 - 349.7]$	$[8.48 - 172.9] \cup [188 - 349]$	$[8.55 - 172.7] \cup [185.8 - 350.3]$
Pattern: $M_{\nu 12} (1 + \chi) + M_{\nu 13} = 0$, and $M_{\nu 22} - M_{\nu 33} = 0$					
$ \chi $			θ		
1σ	2σ	3σ	1σ	2σ	3σ
Degenerate Hierarchy					
$0.0066 - 0.2$	$0.0085 - 0.2$	$0.0049 - 0.2$	$[0.075 - 50.24] \cup [59.11 - 77.88] \cup [129.4 - 233.3] \cup [288.4 - 359.9]$	$[0.20 - 76.48] \cup [108.4 - 242.2] \cup [300.8 - 359.78]$	$[0.1 - 70.91] \cup [85.6 - 254.1] \cup [276.5 - 359.74]$
Normal Hierarchy					
$0.1889 - 0.2$	$0.14 - 0.2$	$0.1 - 0.2$	$[0.48 - 2.17] \cup [357.7 - 359.8]$	$[0.43 - 3.1] \cup [176.7 - 183.4] \cup [356.5 - 359.54]$	$[0.33 - 4.9] \cup [173.2 - 185] \cup [355.1 - 359.75]$
Inverted Hierarchy					
$0.0992 - 0.2$	$0.0814 - 0.2$	$0.06 - 0.2$	$[176.08 - 179.6] \cup [180.4 - 184.12]$	$[0.57 - 4.98] \cup [175.6 - 184.4] \cup [355.6 - 359.65]$	$[0.33 - 6.6] \cup [174.3 - 186.8] \cup [353.8 - 359.87]$
Pattern: $M_{\nu 12} - M_{\nu 13} = 0$, and $M_{\nu 22} (1 + \chi) - M_{\nu 33} = 0$					
$ \chi $			θ		
1σ	2σ	3σ	1σ	2σ	3σ
Degenerate Hierarchy					
$0.0017 - 0.2$	$0.0016 - 0.2$	$0.0025 - 0.2$	$0.30 - 359.75$	$0.08 - 359.84$	$0.15 - 359.65$
Normal Hierarchy					
$0.0729 - 0.2$	$0.0658 - 0.2$	$0.0587 - 0.2$	$[0.17 - 74.5] \cup [285.6 - 359.12]$	$[0.40 - 74.9] \cup [114.3 - 247.4] \cup [286.3 - 359.68]$	$[0.08 - 72.7] \cup [112.4 - 246.9] \cup [285.4 - 359.54]$
Inverted Hierarchy					
$0.0393 - 0.2$	$0.0345 - 0.2$	$0.0426 - 0.2$	$110.1 - 251.33$	$[0.13 - 77.84] \cup [112.5 - 250.5] \cup [283.3 - 359.87]$	$[0.21 - 76.57] \cup [108.3 - 247.6] \cup [283.7 - 359.87]$
Pattern: $M_{\nu 12} + M_{\nu 13} = 0$, and $M_{\nu 22} (1 + \chi) - M_{\nu 33} = 0$					
$ \chi $			θ		
1σ	2σ	3σ	1σ	2σ	3σ
Degenerate Hierarchy					
$0.0112 - 0.2$	$0.0079 - 0.2$	$0.0115 - 0.2$	$1.53 - 359.94$	$0.61 - 358.42$	$0.82 - 359.45$
Normal Hierarchy					
\times	\times	$0.16 - 0.2$	\times	\times	$[0.12 - 19.47] \cup [139.9 - 217.4] \cup [340.8 - 359.9]$
Inverted Hierarchy					
\times	$0.1572 - 0.2$	$0.1047 - 0.2$	\times	$45.7 - 310.22$	$0.03 - 360$

Table 4: The allowed values for $|\chi|$ (pure number) and θ for the patterns of violating exact μ - τ symmetry. All the angles are evaluated in degrees.

8 Singular patterns violating exact μ - τ symmetry

As was the case in the exact symmetry, the violation of exact μ - τ symmetry does not allow for singular neutrino mass matrix. The same analysis and arguments against the viability of the singular patterns having exact μ - τ symmetry in section (5) can be carried out here to show the inviability of the various singular deformed patterns. The numerical study based on scanning all acceptable ranges for the mixing angles and the Dirac phase δ assures the absence of any solution satisfying the mass ratio constraints as expressed in Eq. (30) and Eq. (35). All the relevant formulae for mass ratios are collected in Table (5) in order to ease judging the inviability of patterns. The T_3 and T_4 present in the formulae are the ones defined before in Eq. (65), while T_5 is introduced as

$$T_5 = |\chi|^2 c_y^2 c_\delta + |\chi| [c_\delta c_\theta (4c_y^2 - 1) + s_\theta s_\delta] + 2c_\delta c_{2y}. \quad (72)$$

	$m_1 = 0$	
Pattern	$\frac{m_2}{m_3}$	
C1	$\left \frac{A_3}{A_2} \right \approx \sqrt{\frac{ \chi ^2 s_y^2 + 2 \chi c_\theta s_y (s_y - c_y) + 1 - s_{2y}}{ \chi ^2 c_y^2 + 2 \chi c_\theta s_y (s_y + c_y) + 1 + s_{2y}}} \frac{s_z}{s_x c_x} + O(s_z^2)$	$\left \frac{B_3}{B_2} \right \approx \frac{1}{c_x^2} (1 + 2 t_x t_{2y} c_\delta s_z) + O(s_z^2)$
C2	$\left \frac{A_3}{A_2} \right \approx \sqrt{\frac{ \chi ^2 s_y^2 + 2 \chi c_\theta s_y (s_y + c_y) + 1 + s_{2y}}{ \chi ^2 c_y^2 + 2 \chi c_\theta s_y (c_y - s_y) + 1 - s_{2y}}} \frac{s_z}{s_x c_x} + O(s_z^2)$	$\left \frac{B_3}{B_2} \right \approx \frac{1}{c_x^2} (1 + 2 t_x t_{2y} c_\delta s_z) + O(s_z^2)$
C3	$\left \frac{A_3}{A_2} \right \approx \sqrt{\frac{1 - s_{2y}}{1 + s_{2y}}} \frac{s_z}{s_x c_x} + O(s_z^2)$	$\left \frac{B_3}{B_2} \right \approx \frac{1}{c_x^2} \sqrt{\frac{T_3}{T_4}} \left(1 + \frac{t_x s_{2y} T_5 s_z}{T_4} \right) + O(s_z^2)$
C4	$\left \frac{A_3}{A_2} \right \approx \sqrt{\frac{1 + s_{2y}}{1 - s_{2y}}} \frac{s_z}{s_x c_x} + O(s_z^2)$	$\left \frac{B_3}{B_2} \right \approx \frac{1}{c_x^2} \sqrt{\frac{T_3}{T_4}} \left(1 + \frac{t_x s_{2y} T_5 s_z}{T_4} \right) + O(s_z^2)$
	$m_3 = 0$	
Pattern	$\frac{m_2}{m_1}$	
C1	$\left \frac{A_1}{A_2} \right \approx 1 + \frac{ \chi ^2 s_y c_y c_\delta + \chi [c_\delta c_\theta (s_{2y} - c_{2y}) - s_\theta s_\delta] - c_\delta c_{2y}}{ \chi ^2 c_y^2 + 2 \chi c_\theta c_y (s_y + c_y) + 1 + s_{2y}} \frac{s_z}{s_x c_x} + O(s_z^2)$	$\left \frac{B_1}{B_2} \right \approx t_x^2 \left(1 + \frac{2 t_{2y} c_\delta s_z}{s_x c_x} \right) + O(s_z^2)$
C2	$\left \frac{A_1}{A_2} \right \approx 1 + \frac{ \chi ^2 s_y c_y c_\delta + \chi [c_\delta c_\theta (s_{2y} + c_{2y}) + s_\theta s_\delta] + c_\delta c_{2y}}{ \chi ^2 c_y^2 + 2 \chi c_\theta c_y (c_y - s_y) + 1 - s_{2y}} \frac{s_z}{s_x c_x} + O(s_z^2)$	$\left \frac{B_1}{B_2} \right \approx t_x^2 \left(1 + \frac{2 t_{2y} c_\delta s_z}{s_x c_x} \right) + O(s_z^2)$
C3	$\left \frac{A_1}{A_2} \right \approx 1 - \frac{(1 - s_{2y}) c_\delta s_z}{c_{2y} s_x c_x} + O(s_z^2)$	$\left \frac{B_1}{B_2} \right \approx t_x^2 \left(1 + \frac{T_5 s_{2y} s_z}{T_4 s_x c_x} \right) + O(s_z^2)$
C4	$\left \frac{A_1}{A_2} \right \approx 1 + \frac{(1 + s_{2y}) c_\delta s_z}{c_{2y} s_x c_x} + O(s_z^2)$	$\left \frac{B_1}{B_2} \right \approx t_x^2 \left(1 + \frac{T_5 s_{2y} s_z}{T_4 s_x c_x} \right) + O(s_z^2)$

Table 5: The approximate mass ratio formulae for the singular light neutrino mass violating exact $\mu - \tau$ symmetry. The formulae are calculated in terms of A's and B's coefficients

9 Exact $\mu - \tau$ symmetry and realizations of the perturbed textures

We study now in detail how the perturbed textures can arise assuming an exact $\mu - \tau$ symmetry at the Lagrangian level but at the expense of introducing new matter fields and symmetries. To fix the ideas, let's take the C1 pattern put in the form:

$$M_\nu = \begin{pmatrix} A & B & B(1 + \chi) \\ B & C & D \\ B(1 + \chi) & D & C \end{pmatrix}. \quad (73)$$

The exact $\mu - \tau$ symmetry (the S symmetry) corresponding to this pattern is given by the matrix

$$S = \begin{pmatrix} 1 & 0 & 0 \\ 0 & 0 & 1 \\ 0 & 1 & 0 \end{pmatrix} \quad (74)$$

in that we have $S^2 = 1$ and

$$\left\{ \left(M = M^T \right) \wedge \left[S^T \cdot M \cdot S = M \right] \right\} \Leftrightarrow \left[\exists A, B, C, D : M = \begin{pmatrix} A & B & B \\ B & C & D \\ B & D & C \end{pmatrix} \right], \quad (75)$$

We shall need also the following relations:

$$\left\{ \left(M = M^T \right) \wedge \left[S^T \cdot M \cdot S = -M \right] \right\} \Leftrightarrow \left[\exists B, C : M = \begin{pmatrix} 0 & B & -B \\ B & C & 0 \\ -B & 0 & -C \end{pmatrix} \right], \quad (76)$$

$$\left[S^T \cdot M \cdot S = M \right] \Leftrightarrow \left[\exists A, B, C, D : M = \begin{pmatrix} A & B & B \\ E & C & D \\ E & D & C \end{pmatrix} \right], \quad (77)$$

$$\left[S^T \cdot M \cdot S = -M \right] \Leftrightarrow \left[\exists B, C, D : M = \begin{pmatrix} 0 & B & -B \\ E & C & D \\ -E & -D & -C \end{pmatrix} \right], \quad (78)$$

$$\left[S \cdot M = M \right] \Leftrightarrow \left[\exists A, B, C, D, E, F : M = \begin{pmatrix} A & B & C \\ D & E & F \\ D & E & F \end{pmatrix} \right] \quad (79)$$

We shall achieve the texture of Eq. 73 using both types II and I of the seesaw mechanism.

9.1 Type II-seesaw

In the type II seesaw [40] mechanism, we show now how one can reach the desired form by assuming a flavor symmetry of the form $S \times Z_2$ and by having three Higgs triplets for the neutrino mass matrix and three Higgs doublets for the charged lepton mass matrix.

9.1.1 Matter content and symmetries

First, we extend the SM by introducing three $SU(2)_L$ scalar triplets H_a , ($a = 1, 2, 3$),

$$H_a \equiv [H_a^{++}, H_a^+, H_a^0]. \quad (80)$$

In addition to the S symmetry, we introduce another Z_2 symmetry, and we assume the following transformations:

$$L \xrightarrow{S} SL \quad , \quad L \xrightarrow{Z_2} \text{diag}(1, -1, -1)L \quad (81)$$

$$H \xrightarrow{S} \text{diag}(1, 1, -1)H \quad , \quad H \xrightarrow{Z_2} \text{diag}(1, -1, -1)H \quad (82)$$

where the $L^T = (L_1, L_2, L_3)$, $H^T = (H_1, H_2, H_3)$ with L_i 's, ($i = 1, 2, 3$) are the components of the i^{th} -family LH lepton doublets (we shall adopt this notation of 'vectors' in flavor space even for other fields, like l^c , ν_R and ϕ, \dots). Note that the assignments of L_2, L_3 should be the same under Z_2 as the S symmetry interchanges them, otherwise the factor subgroups S and Z_2 do not commute. For this reason, the S -charges of H_2, H_3 are allowed to be different because Z_2 acts on H diagonally. There will be also the RH charged lepton singlets and the Higgs fields responsible for the charged lepton mass matrix.

9.1.2 Neutrino mass matrix

The Yukawa interaction relevant for neutrino mass has the form,

$$\mathcal{L}_{H,L} = \sum_{i,j=1}^3 \sum_{a=1}^3 G_{ij}^a [H_a^0 \nu_{Li}^T \mathcal{C} \nu_{Lj} + H_a^+ (\nu_{Li}^T \mathcal{C} l_{Lj} + l_{Lj}^T \mathcal{C} \nu_{Li}) + H_a^{++} l_{Li}^T \mathcal{C} l_{Lj}], \quad (83)$$

where G_{ij}^a are Yukawa coupling constants, the indices i, j are flavor ones, and \mathcal{C} is the charge conjugation matrix.

The field H_a^0 can get a small vacuum expectation value (vev), $\langle H_a^0 \rangle_0 = v_a$ leading to a Majorana neutrino mass matrix,

$$M_{\nu ij} = \sum_{a=1}^3 G_{ij}^a \langle H_a^0 \rangle_0. \quad (84)$$

The smallness of the vev $\langle H_a^0 \rangle_0$ is due to the largeness of the triplet scalar mass scale[40].

The bilinear of $\nu_{Li} \nu_{Lj}$ relevant for Majorana mass matrix transforms, via Eq. 81, under Z_2 as:

$$\nu_{Li} \nu_{Lj} \xrightarrow{Z_2} B \begin{pmatrix} 1 & -1 & -1 \\ -1 & 1 & 1 \\ -1 & 1 & 1 \end{pmatrix}, \quad \text{meaning: } \nu_{Li} \nu_{Lj} \xrightarrow{Z_2} Z_2(\nu_{Li} \nu_{Lj}) = B_{ij} \nu_{Li} \nu_{Lj} (\text{no sum}) \quad (85)$$

Thus we have:

$$\left. \begin{aligned} S^T G^1 S &= G^1, G^{1T} = G^1 \\ G_{ij}^1 Z_2(H_1) Z_2(\nu_{Li} \nu_{Lj}) &= G_{ij}^1 H_1 \nu_{Li} \nu_{Lj} (\text{no sum}) \end{aligned} \right\} \xrightarrow{\text{Eqs.75,82,85}} G^1 = \begin{pmatrix} A^1 & 0 & 0 \\ 0 & C^1 & D^1 \\ 0 & D^1 & C^1 \end{pmatrix} \quad (86)$$

$$\left. \begin{aligned} S^T G^2 S &= G^2, G^{2T} = G^2 \\ G_{ij}^2 Z_2(H_2) Z_2(\nu_{Li} \nu_{Lj}) &= G_{ij}^2 H_2 \nu_{Li} \nu_{Lj} (\text{no sum}) \end{aligned} \right\} \xrightarrow{\text{Eqs.75,82,85}} G^2 = \begin{pmatrix} 0 & B^2 & B^2 \\ B^2 & 0 & 0 \\ B^2 & 0 & 0 \end{pmatrix} \quad (87)$$

The two Higgs fields H_1, H_2 generate the unperturbed texture, whereas the perturbation is generated by the field H_3 :

$$\left. \begin{aligned} S^T G^3 S &= -G^3, G^{3T} = G^3 \\ G_{ij}^3 Z_2(H_3) Z_2(\nu_{Li} \nu_{Lj}) &= G_{ij}^3 H_3 \nu_{Li} \nu_{Lj} (\text{no sum}) \end{aligned} \right\} \xrightarrow{\text{Eqs.76,82,85}} G^3 = \begin{pmatrix} 0 & B^3 & -B^3 \\ B^3 & 0 & 0 \\ -B^3 & 0 & 0 \end{pmatrix} \quad (88)$$

The mass matrix we get is of the form:

$$M_{\nu} = \begin{pmatrix} v_1 A^1 & v_2 B^2 + v_3 B^3 & v_2 B^2 - v_3 B^3 \\ v_2 B^2 + v_3 B^3 & v_1 C^1 & v_1 D^1 \\ v_2 B^2 - v_3 B^3 & v_1 D^1 & v_1 C^1 \end{pmatrix}. \quad (89)$$

Thus if the Yukawa couplings are all of the same order while the vevs satisfy $v_2 \gg v_3$ we get the desired form of the pattern $C1$ (Eq. 73) with $\chi = \frac{-2v_3 B^3}{v_2 B^2 + v_3 B^3}$.

9.1.3 Charged lepton mass matrix – flavor basis

We need here to extend the symmetry to the charged lepton sector and arrange the couplings in order to be in the ‘flavor basis’ where the charged lepton mass matrix is diagonal. For this we present three possible options.

1. Just the SM Higgs

We have the usual Yukawa coupling term

$$\mathcal{L}_1 = Y_{ij} \bar{L}_i \Phi l_j^c \quad (90)$$

We assume the SM Higgs Φ is singlet under the flavor symmetry.

$$\Phi \xrightarrow{S} \Phi \quad , \quad \Phi \xrightarrow{Z_2} \Phi \quad (91)$$

and present two scenarios for the RH charged lepton singlets l_j^c transformation under $S \times Z_2$ as follows.

- l_j^c transforms similarly as L

We assume:

$$l^c \xrightarrow{S} S l^c \quad , \quad l^c \xrightarrow{Z_2} \text{diag}(1, -1, -1) l^c \quad (92)$$

We get via Eqs. (81,91 and 92) then:

$$S^T Y S = Y \quad , \quad \bar{L}_i l_j^c \xrightarrow{Z_2} \begin{pmatrix} 1 & -1 & -1 \\ -1 & 1 & 1 \\ -1 & 1 & 1 \end{pmatrix} \quad (93)$$

which would lead, upon acquiring a vev v for the SM Higgs, to a charged lepton mass matrix of the form (see Eqs. 77, 93):

$$M_l = v \begin{pmatrix} A & 0 & 0 \\ 0 & C & D \\ 0 & D & C \end{pmatrix} \Rightarrow M_l M_l^\dagger = v^2 \begin{pmatrix} |A|^2 & 0 & 0 \\ 0 & |C|^2 + |D|^2 & 2\Re(CD^*) \\ 0 & 2\Re(CD^*) & |C|^2 + |D|^2 \end{pmatrix}. \quad (94)$$

Thus we need to perform a rotation across the 1st-axis by an angle $\theta_y = \pi/4$ in order to diagonalize the squared charged lepton mass matrix and be in the flavor basis. Thus, this option is not interesting since it spoils the neutrino mixing predictions carried out in the flavor basis.

- l_j^c is singlet under flavor symmetry

We assume:

$$l^c \xrightarrow{S} l^c \quad , \quad l^c \xrightarrow{Z_2} l^c \quad (95)$$

We get via Eqs. (81,91 and 95) then:

$$S Y = Y \quad , \quad \bar{L}_i l_j^c \xrightarrow{Z_2} \begin{pmatrix} 1 & 1 & 1 \\ -1 & -1 & -1 \\ -1 & -1 & -1 \end{pmatrix} \quad (96)$$

which would lead, upon acquiring a vev v for the SM Higgs, to a charged lepton mass matrix of the form (see Eqs. 79, 96):

$$M_l = v \begin{pmatrix} A & B & C \\ 0 & 0 & 0 \\ 0 & 0 & 0 \end{pmatrix} \Rightarrow M_l M_l^\dagger = v^2 \begin{pmatrix} |A|^2 + |B|^2 + |C|^2 & 0 & 0 \\ 0 & 0 & 0 \\ 0 & 0 & 0 \end{pmatrix}. \quad (97)$$

The squared mass matrix is diagonal, but it predicts two vanishing eigen masses for the 2nd and 3rd families which is not acceptable experimentally.

2. Three SM-like Higgs doublets

We extend the SM to include three scalar doublets ϕ_k playing the role of the ordinary SM-Higgs field. The Lagrangian responsible for the charged lepton mass is given by:

$$\mathcal{L}_2 = f_{ik}^j \bar{L}_i \phi_k l_j^c \quad (98)$$

We assume the Higgs fields ϕ_k , $k = 1, 2, 3$ transform as L_i under $S \times Z_2$:

$$\phi \xrightarrow{S} S \phi \quad , \quad \phi \xrightarrow{Z_2} \text{diag}(1, -1, -1) \phi \quad (99)$$

Equally, the RH charged leptons are supposed to transform as singlets under S :

$$l^c \xrightarrow{S} l^c \quad (100)$$

whereas we present two scenarios for their transformations under Z_2 as follows.

- l_j^c transforms similarly as L under Z_2

We assume

$$l^c \xrightarrow{Z_2} \text{diag}(1, -1, -1)l^c \quad (101)$$

We get via Eqs. (81,99, 100 and 101) then:

$$S^T f^{(j)} S = f^{(j)} \quad , \quad \bar{L}_i \phi_k \xrightarrow{Z_2} \begin{pmatrix} 1 & -1 & -1 \\ -1 & 1 & 1 \\ -1 & 1 & 1 \end{pmatrix} \quad (102)$$

where $f^{(j)}$ is the matrix whose $(i, k)^{th}$ -entry is the Yukawa coupling f_{ik}^j . Then, Eqs. (77, 101 and 102) lead to the following forms of the Yukawa coupling matrices:

$$f^{(1)} = \begin{pmatrix} A^1 & 0 & 0 \\ 0 & C^1 & D^1 \\ 0 & D^1 & C^1 \end{pmatrix}, f^{(2)} = \begin{pmatrix} 0 & B^2 & B^2 \\ E^2 & 0 & 0 \\ E^2 & 0 & 0 \end{pmatrix}, f^{(3)} = \begin{pmatrix} 0 & B^3 & B^3 \\ E^3 & 0 & 0 \\ E^3 & 0 & 0 \end{pmatrix} \quad (103)$$

If there is cute hierarchy in the vevs: $v_3 \gg v_1, v_2$, say, we get, for real entries, a charged lepton mass matrix of the form

$$M_l = v_3 \begin{pmatrix} 0 & B^2 & B^3 \\ D^1 & 0 & 0 \\ C^1 & 0 & 0 \end{pmatrix} \quad (104)$$

We see that this choice of Z_2 -charge assignments for the RH lepton singlets leads to one vanishing mass, which is excluded by experiment. Thus we turn to the other choice which would prove capable of producing the charged lepton mass spectrum.

- l_j^c transforms differently from L under Z_2

We assume

$$l^c \xrightarrow{Z_2} \text{diag}(1, 1, -1)l^c \quad (105)$$

We get the same Eq. (102), but Eq. (105) leads now to:

$$f^{(1)} = \begin{pmatrix} A^1 & 0 & 0 \\ 0 & C^1 & D^1 \\ 0 & D^1 & C^1 \end{pmatrix}, f^{(2)} = \begin{pmatrix} A^2 & 0 & 0 \\ 0 & C^2 & D^2 \\ 0 & D^2 & C^2 \end{pmatrix}, f^{(3)} = \begin{pmatrix} 0 & B^3 & B^3 \\ E^3 & 0 & 0 \\ E^3 & 0 & 0 \end{pmatrix} \quad (106)$$

The hierarchy ($v_3 \gg v_1, v_2$) would now lead to the following form for the charged lepton mass matrix:

$$M_l = v_3 \begin{pmatrix} 0 & 0 & B^3 \\ D^1 & D^2 & 0 \\ C^1 & C^2 & 0 \end{pmatrix} \Rightarrow M_l M_l^\dagger = v_3^2 \begin{pmatrix} |\mathbf{B}|^2 & 0 & 0 \\ 0 & |\mathbf{D}|^2 & \mathbf{D} \cdot \mathbf{C} \\ 0 & \mathbf{C} \cdot \mathbf{D} & |\mathbf{C}|^2 \end{pmatrix}, \quad (107)$$

where $\mathbf{B} = (0, 0, B^3)^T$, $\mathbf{D} = (D^1, D^2, 0)^T$ and $\mathbf{C} = (C^1, C^2, 0)^T$, and where the dot product is defined as $\mathbf{D} \cdot \mathbf{C} = \sum_{i=1}^{i=3} D^i C^{i*}$. Now, one can adjust the Yukawa couplings so that to require an infinitesimal rotation in order to diagonalize the squared charged lepton mass matrix and

be in the flavor basis. In fact, let us just assume the magnitudes of the three vectors coming in ratios comparable to the lepton mass ratios:

$$\frac{|\mathbf{B}|}{|\mathbf{C}|} \equiv \lambda_e \sim \frac{m_e}{m_\tau} = 2.8 \times 10^{-4} \quad , \quad \frac{|\mathbf{D}|}{|\mathbf{C}|} \equiv \lambda_\mu \sim \frac{m_\mu}{m_\tau} = 5.9 \times 10^{-2}, \quad (108)$$

Then it is easy to see that the matrix:

$$U(\theta, \alpha, \beta) = \begin{pmatrix} 1 & 0 & 0 \\ 0 & c_\theta e^{-i\alpha} & s_\theta e^{-i\beta} \\ 0 & -s_\theta e^{-i\alpha} & c_\theta e^{-i\beta} \end{pmatrix} : \quad (109)$$

$$\alpha - \beta = \arg(\mathbf{D} \cdot \mathbf{C}) \quad , \quad \tan 2\theta = \frac{2\mathbf{D} \cdot \mathbf{C}}{|\mathbf{D}|^2 - |\mathbf{C}|^2} \simeq 2 \frac{|\mathbf{D}|}{|\mathbf{C}|} \cos \psi \quad (110)$$

where ψ is the angle between the two complex vectors \mathbf{D} and \mathbf{C} , defined by $\cos \psi = \mathbf{D} \cdot \mathbf{C} / (|\mathbf{D}| \cdot |\mathbf{C}|)$, does diagonalize $M_l M_l^\dagger$. Note that one can absorb the individual phases α, β , using the freedom of multiplying the unitary diagonalizing matrix by a diagonal phase matrix, which would leave us with only one ‘physical’ phase $\alpha - \beta$:

$$U(\theta, \alpha, \beta) = \begin{pmatrix} 1 & 0 & 0 \\ 0 & c_\theta & s_\theta e^{-i(\beta-\alpha)} \\ 0 & -s_\theta e^{i(\beta-\alpha)} & c_\theta \end{pmatrix} \quad (111)$$

Thus, we are in the flavor basis, as required, up to an infinitesimal rotation of angle less than 10^{-2} (See Eqs. 108 and 110).

3. SM plus three Higgs singlets

One might keep the SM Higgs doublet Φ , with the same flavor transformations of Eq. (91) but add three Higgs singlets Δ_k so that to contribute to the charged lepton mass through dimension-5 operators. The Lagrangian responsible for the charged lepton mass is given by:

$$\mathcal{L}_4 = \mathcal{L}_1 + \mathcal{L}_3 = Y_{ij} \bar{L}_i \Phi l_j^c + \frac{g_{ik}^j}{\Lambda} \bar{L}_i \Phi \Delta_k l_j^c \quad (112)$$

where Λ is a mass high scale characterizing the Higgs singlets. We assume the Higgs singlet fields Δ_k , $k = 1, 2, 3$ transform as L_i under $S \times Z_2$:

$$\Delta \xrightarrow{S} S\Delta \quad , \quad \Delta \xrightarrow{Z_2} \text{diag}(1, -1, -1)\Delta \quad (113)$$

As in the previous enumeration, the RH charged leptons are supposed to be singlets under S (Eq. 100), whereas for Z_2 we have the following options:

- l_j^c transforms similarly as L under Z_2

We have thus Eq.(101). The invariance of \mathcal{L}_1 implies

$$SY = Y \quad , \quad \bar{L}_i l_j^c \xrightarrow{Z_2} \begin{pmatrix} 1 & -1 & -1 \\ -1 & 1 & 1 \\ -1 & 1 & 1 \end{pmatrix} \quad (114)$$

This leads, when Φ acquires a vev, to a contribution to the mass matrix (see Eqs. 79, 93):

$$M_1 = \begin{pmatrix} a & 0 & 0 \\ 0 & e & f \\ 0 & e & f \end{pmatrix} \quad (115)$$

Eq. (113) would lead, exactly as the three Higgs doublets did in the previous enumeration, to a mass contribution M_2 of the form of Eq. 104 when the Higgs singlets acquire vevs (δ_k), with the hierarchy $\delta_3 \gg \delta_1, \delta_2$. Thus we get the charged lepton mass matrix in the form:

$$M_l = M_1 + M_2 = \begin{pmatrix} a & B^2 & B^3 \\ D^1 & e & f \\ C^1 & e & f \end{pmatrix} \quad (116)$$

with the condition that $D^1 \neq C^1$ in order not to make the determinant of the matrix equal to zero implying a vanishing mass.

- l_j^c **transforms differently from L under Z_2**

We have thus Eq.(105). The invariance of \mathcal{L}_1 implies:

$$SY = Y \quad , \quad \bar{L}_i l_j^c \stackrel{Z_2}{\sim} \begin{pmatrix} 1 & 1 & -1 \\ -1 & -1 & 1 \\ -1 & -1 & 1 \end{pmatrix} \quad (117)$$

so when Φ acquires a vev we get a contribution to the mass matrix (see Eqs. 79, 117):

$$M_1 = \begin{pmatrix} a & b & 0 \\ 0 & 0 & f \\ 0 & 0 & f \end{pmatrix} \quad (118)$$

Eq. (113) would lead, exactly as the three Higgs doublets did in the previous case, to a mass contribution M_2 of the form of Eq. 107 when the Higgs singlets acquire vevs (δ_k), with the hierarchy $\delta_3 \gg \delta_1, \delta_2$. Thus we get the charged lepton mass matrix in the form:

$$M_l = M_1 + M_2 = \begin{pmatrix} a & b & B^3 \\ D^1 & D^2 & f \\ C^1 & C^2 & f \end{pmatrix} \quad (119)$$

- In both previous items we get a charged lepton mass matrix of the form

$$M_l = \begin{pmatrix} \mathbf{A}^T \\ \mathbf{B}^T \\ \mathbf{C}^T \end{pmatrix} \quad (120)$$

adjustable so that the three vectors are linearly independent making the mass matrix invertible. The discussion in [41] on the charged lepton mass matrix of the same form showed the possibility to adjust Yukawa couplings in order to get the charged lepton mass hierarchy, and then automatically the working basis will become the flavor basis up to order λ_μ . We shall not repeat the same analysis here, but just note that in case the parameters a, b, f (corresponding to \mathcal{L}_1) are negligible compared to B, C, D (related to \mathcal{L}_3) then the last item (Eq. 119) is similar to the last item of the past enumeration (Eq. 107), where we showed explicitly the charged lepton mass diagonalizing matrix being an infinitesimal rotation, which allows to consider the matrices as being those in the flavor basis, with a good approximation.

Before we finish this subsection, we note that there is an advantage for using the type-II seesaw mechanism in that the flavor changing neutral current due to the triplet is highly suppressed because of the heaviness of the triplet mass scale, or equivalently the smallness of the neutrino masses.

9.2 Type-I seesaw

We proceed now to find a realization of the perturbed texture of pattern C1 (Eq. 73) in type-I seesaw mechanism where the effective neutrino mass matrix (M_ν) is expressed in terms of the Dirac neutrino mass matrix (M_D) and the RH Majorana neutrino mass matrix (M_R) through:

$$M_\nu = M_D M_R^{-1} M_D^T \quad (121)$$

For the flavor symmetry, we start by adding a new Z_2 symmetry (called Z'_2) to the flavor symmetry of the type II case, but we shall see that it is not enough to achieve the desired form, and needs to be expanded to a larger group (say to $S \times Z_8$) for this.

9.2.1 $S \times Z_2 \times Z'_2$ -flavor symmetry

We consider here a minimal extension to the flavor group of the type II seesaw by adding a new Z_2 -symmetry so that to get the group $(Z_2)^3$.

1. Matter content and symmetry transformations

We have three SM-like Higgs doublets $(\phi_i, i = 1, 2, 3)$ which would give mass to the charged leptons and another three Higgs doublets $(\phi'_i, i = 1, 2, 3)$ for the Dirac neutrino mass matrix. The RH neutrinos are denoted by $(\nu_{Ri}, i = 1, 2, 3)$. These fields transform as follows.

$$\nu_R \xrightarrow{Z'_2} -\nu_R, \quad \phi' \xrightarrow{Z'_2} -\phi' \quad (122)$$

$$L \xrightarrow{Z'_2} L, \quad l^c \xrightarrow{Z'_2} l^c, \quad \phi \xrightarrow{Z'_2} \phi, \quad (123)$$

$$\nu_R \xrightarrow{Z_2} \text{diag}(1, -1, -1)\nu_R, \quad \phi' \xrightarrow{Z_2} \text{diag}(1, -1, -1)\phi' \quad (124)$$

$$L \xrightarrow{Z_2} \text{diag}(1, -1, -1)L, \quad l^c \xrightarrow{Z_2} \text{diag}(1, 1, -1)l^c, \quad \phi \xrightarrow{Z_2} \text{diag}(1, -1, -1)\phi, \quad (125)$$

$$\nu_R \xrightarrow{S} S\nu_R, \quad \phi' \xrightarrow{S} \text{diag}(1, 1, -1)\phi' \quad (126)$$

$$L \xrightarrow{S} SL, \quad l^c \xrightarrow{S} l^c, \quad \phi \xrightarrow{S} S\phi, \quad (127)$$

2. Charged lepton mass matrix-flavor basis

As was the case of type-II seesaw with three SM-like Higgs doublets and where the RH charged lepton singlets transform differently from L under Z_2 , the Lagrangian responsible for the charged lepton mass is given by Eq. (98). The Z'_2 does not play a role here, since all the fields involved are singlets under it, except for the fact that it does forbid the trilinear coupling between ϕ', L and l^c . Again, assuming a hierarchy in the Higgs ϕ 's fields vevs ($v_3 \gg v_2, v_1$) we end up with a charged lepton mass matrix of the form (Eq. 107) which can be adjusted to be in the flavor basis to a good approximation.

3. Dirac neutrino mass matrix

The Lagrangian responsible for the neutrino mass matrix is

$$\mathcal{L}_D = g_{ij}^k \bar{L}_i \tilde{\phi}'_k \nu_{Rj}, \quad \text{where } \tilde{\phi}' = i\sigma_2 \phi'^* \quad (128)$$

This lagrangian is clearly invariant under Z'_2 (see Eq. 122) which forces the existence of ϕ' rather than ϕ in \mathcal{L}_D . For the $S \times Z_2$ factor, we get via Eqs. (124,125, 126 and 127) then:

$$S^T g^{(k=1,2)} S = g^{(k=1,2)}, \quad S^T g^{(k=3)} S = -g^{(k=3)}, \quad \bar{L}_i \nu_{Rj} \xrightarrow{Z_2} \begin{pmatrix} 1 & -1 & -1 \\ -1 & 1 & 1 \\ -1 & 1 & 1 \end{pmatrix} \quad (129)$$

where $g^{(k)}$ is the matrix whose $(i, j)^{th}$ -entry is the Yukawa coupling g_{ij}^k . Then, Eqs. (77, 78, 124 and 129) lead to the following forms of the Yukawa coupling matrices:

$$g^{(1)} = \begin{pmatrix} A^1 & 0 & 0 \\ 0 & C^1 & D^1 \\ 0 & D^1 & C^1 \end{pmatrix}, \quad g^{(2)} = \begin{pmatrix} 0 & B^2 & B^2 \\ E^2 & 0 & 0 \\ E^2 & 0 & 0 \end{pmatrix}, \quad g^{(3)} = \begin{pmatrix} 0 & B^3 & -B^3 \\ E^3 & 0 & 0 \\ -E^3 & 0 & 0 \end{pmatrix} \quad (130)$$

Upon acquiring vevs ($v'_i, i = 1, 2, 3$) for the Higgs fields (ϕ'_i), we get the following Dirac neutrino mass matrix:

$$M_D = \sum_{k=1}^3 v'_k g^{(k)} = \begin{pmatrix} A_D & B_D & B_D(1 + \alpha) \\ E_D & C_D & D_D \\ E_D(1 + \beta) & D_D & C_D \end{pmatrix} \quad (131)$$

with

$$\alpha = \frac{-2v'_3 B^3}{v'_2 B^2 + v'_3 B^3} \quad , \quad \beta = \frac{-2v'_3 E^3}{v'_2 E^2 + v'_3 E^3} \quad (132)$$

If the vevs satisfy $v'_3 \ll v'_2$ and the Yukawa couplings are of the same order then we get perturbative parameters $\alpha, \beta \ll 1$.

4. Majorana neutrino mass matrix

The mass term is directly present in the Lagrangian

$$\mathcal{L}_R = M_{Rij} \nu_{Ri} \nu_{Rj} \quad (133)$$

It is invariant under Z'_2 . Then Eqs. (126,124) lead to:

$$S^T M_R S = M_{R, \nu_{Ri} \nu_{Rj}} \xrightarrow{Z_2} \begin{pmatrix} 1 & -1 & -1 \\ -1 & 1 & 1 \\ -1 & 1 & 1 \end{pmatrix} \xrightarrow{\text{Eq. 75}} M_R = \begin{pmatrix} A_R & 0 & 0 \\ 0 & C_R & D_R \\ 0 & D_R & C_R \end{pmatrix} \quad (134)$$

5. Effective neutrino mass matrix

One can see by direct computation that plugging Eqs. (131,134) in the seesaw formula (Eq. 121) would result in an effective neutrino mass matrix of the form:

$$M_\nu = \begin{pmatrix} M_{\nu 11} & M_{\nu 12} & M_{\nu 12}(1 + \chi) \\ M_{\nu 12} & M_{\nu 22} & M_{\nu 23} \\ M_{\nu 12}(1 + \chi) & M_{\nu 23} & M_{\nu 22}(1 + \xi) \end{pmatrix} \quad (135)$$

where $(Y = A, B, C, D, E)$

$$\chi = \chi(\alpha, \beta, Y_D, Y_R), \quad \xi = \xi(\beta, Y_D, Y_R) : \beta = 0 \Rightarrow \xi = 0 \quad (136)$$

Thus, in general, we do not get the desired $C1$ -pattern form (Eq. 73) corresponding to $\xi = 0$. However, for some choices of the Yukawa couplings satisfying $E^3 = 0$ we get this form (see Eq. 132), with χ , as α , is a small parameter for moderate values of Yukawa couplings.

9.2.2 $S \times Z_8$ -flavor symmetry

In order to get a realization of the $C1$ pattern form with no need to tune the Yukawa couplings, we extend the flavor symmetry to be $S \times Z_8$.

1. Matter content and symmetry transformations

The matter spectrum consists of three SM-like Higgs doublets $(\phi_i, i = 1, 2, 3)$ responsible for the charged lepton masses, and of four Higgs doublets $(\phi'_j, j = 1, 2, 3, 4)$ giving rise when acquiring a vev to Dirac neutrino mass matrix, and, as before, of left doublets $(L_i, i = 1, 2, 3)$, RH charged singlets $(l_j^c, j = 1, 2, 3)$ and RH neutrinos $(\nu_{Rj}, j = 1, 2, 3)$. We introduce also two Higgs singlet scalars $(\Delta_k, k = 1, 2)$ related to Majorana neutrino mass matrix. We denote the octic root of the unity by $w = e^{\frac{i\pi}{4}}$. The fields transform under the flavor symmetry as follows.

$$L \xrightarrow{S} SL, \quad l^c \xrightarrow{S} l^c, \quad \phi \xrightarrow{S} S\phi, \quad (137)$$

$$\nu_R \xrightarrow{S} S\nu_R, \quad \phi' \xrightarrow{S} \text{diag}(1, 1, 1, -1)\phi', \quad \Delta \xrightarrow{S} \Delta \quad (138)$$

$$L \xrightarrow{Z_8} \text{diag}(1, -1, -1)L, \quad l^c \xrightarrow{Z_8} \text{diag}(1, 1, -1)l^c, \quad \phi \xrightarrow{Z_8} \text{diag}(1, -1, -1)\phi, \quad (139)$$

$$\nu_R \xrightarrow{Z_8} \text{diag}(w, w^3, w^3)\nu_R, \quad \phi' \xrightarrow{Z_8} \text{diag}(w, w^3, w^7, w^3)\phi', \quad \Delta \xrightarrow{Z_8} \text{diag}(w^6, w^2)\Delta \quad (140)$$

Note here that we have the following transformation rule for $\tilde{\phi}' \equiv i\sigma_2 \phi'^*$:

$$\tilde{\phi}' \xrightarrow{S} \text{diag}(1, 1, 1, -1)\tilde{\phi}' \quad , \quad \tilde{\phi}' \xrightarrow{Z_8} \text{diag}(w^7, w^5, w, w^5)\tilde{\phi}' \quad (141)$$

2. Charged lepton mass matrix-flavor basis

As in the previous case of $S \times Z_2 \times Z'_2$ -flavor symmetry, the charged lepton mass Lagrangian is given again by Eq. (98). Since the transformations of the involved fields (L, l^c, ϕ) are identical under S in both flavor symmetry groups and are equally the same under Z_8 (in $S \times Z_8$) compared to Z_2 (in $S \times Z_2 \times Z'_2$), we end up, assuming again a hierarchy in the Higgs ϕ 's fields vevs ($v_3 \gg v_2, v_1$), with a charged lepton mass matrix of the form (Eq. 107) adjustable to be approximately in the flavor basis. Note also here that no terms of the form $f_{ij}^{k'} \bar{L}_i \phi'_k l_j^c$ can exist since we have:

$$\bar{L}_i l_j^c \stackrel{Z_8}{\sim} \begin{pmatrix} 1 & 1 & -1 \\ -1 & -1 & 1 \\ -1 & -1 & 1 \end{pmatrix} \stackrel{\text{Eq.140}}{\implies} \nexists i, j, k : \bar{L}_i \phi'_k l_j^c = Z_8(\bar{L}_i \phi'_k l_j^c) \quad (142)$$

3. Dirac neutrino mass matrix

The Lagrangian responsible for the neutrino mass matrix is again given by Eq. (128). By means of Eqs. (137, 138, 139, 140 and 141) we have:

$$S^T g^{(k=1,2)} S = g^{(k=1,2,3)} \quad , \quad S^T g^{(k=4)} S = -g^{(k=4)}, \bar{L}_i \nu_{Rj} \stackrel{Z_8}{\sim} \begin{pmatrix} w & w^3 & w^3 \\ w^5 & w^7 & w^7 \\ w^5 & w^7 & w^7 \end{pmatrix} \quad (143)$$

where, as before, $g^{(k)}$ is the matrix whose $(i, j)^{th}$ -entry is the Yukawa coupling g_{ij}^k . Then, Eqs. (77, 78 and 141 and 143) impose the following forms on the Yukawa coupling matrices:

$$g^{(1)} = \begin{pmatrix} A^1 & 0 & 0 \\ 0 & 0 & 0 \\ 0 & 0 & 0 \end{pmatrix}, g^{(2)} = \begin{pmatrix} 0 & B^2 & B^2 \\ 0 & 0 & 0 \\ 0 & 0 & 0 \end{pmatrix}, g^{(3)} = \begin{pmatrix} 0 & 0 & 0 \\ 0 & C^3 & D^3 \\ 0 & D^3 & C^3 \end{pmatrix}, g^{(4)} = \begin{pmatrix} 0 & B^4 & -B^4 \\ 0 & 0 & 0 \\ 0 & 0 & 0 \end{pmatrix} \quad (144)$$

When the Higgs fields (ϕ'_i) get vevs $(v'_i, i = 1, 2, 3, 4)$, we obtain the following Dirac neutrino mass matrix:

$$M_D = \sum_{k=1}^{k=4} v'_k g^{(k)} = \begin{pmatrix} A_D & B_D & B_D(1 + \alpha) \\ 0 & C_D & D_D \\ 0 & D_D & C_D \end{pmatrix} \quad (145)$$

with

$$\alpha = \frac{-2v'_4 B^4}{v'_2 B^2 + v'_4 B^4} \quad (146)$$

If the vevs satisfy $v'_4 \ll v'_2$ and the Yukawa couplings are of the same order then we get a perturbative parameter $\alpha \ll 1$.

4. Majorana neutrino mass matrix

The mass term is generated from the Lagrangian

$$\mathcal{L}_R = h_{ij}^k \Delta_k \nu_{Ri} \nu_{Rj} \quad (147)$$

Under Z_8 we have the bilinear:

$$\nu_{Ri} \nu_{Rj} \stackrel{Z_8}{\sim} \begin{pmatrix} w^2 & w^4 & w^4 \\ w^4 & w^6 & w^6 \\ w^4 & w^6 & w^6 \end{pmatrix} \stackrel{\text{Eq.140}}{\implies} \mathcal{L}_R = h_{11}^1 \Delta_1 \nu_{R1} \nu_{R1} + h_{11}^2 \Delta_2 \nu_{R2} \nu_{R2} + h_{23}^2 \Delta_2 \nu_{R2} \nu_{R3} + h_{32}^2 \Delta_2 \nu_{R3} \nu_{R2} + h_{33}^2 \Delta_2 \nu_{R3} \nu_{R3} \quad (148)$$

If we call $h^{(k)}$ the matrix whose $(i, j)^{th}$ -entry is the coupling h_{ij}^k then we have (the cross sign denote a non-vanishing entry):

$$h^{(1)} = \begin{pmatrix} \times & 0 & 0 \\ 0 & 0 & 0 \\ 0 & 0 & 0 \end{pmatrix} \quad , \quad h^{(2)} = \begin{pmatrix} 0 & 0 & 0 \\ 0 & \times & \times \\ 0 & \times & \times \end{pmatrix} \quad (149)$$

Then Eq. (138) leads to:

$$S^T h^{(k)} S = h^{(k)}, \quad \xrightarrow{\text{Eqs. 75, 149}} \quad h^{(1)} = \begin{pmatrix} a_R & 0 & 0 \\ 0 & 0 & 0 \\ 0 & 0 & 0 \end{pmatrix}, \quad h^{(2)} = \begin{pmatrix} 0 & 0 & 0 \\ 0 & c_R & d_R \\ 0 & d_R & c_R \end{pmatrix} \quad (150)$$

Thus when the Higgs singlets Δ acquires vevs (δ_1^0, δ_2^0) we get the Majorana neutrino mass matrix:

$$M_R = \sum_{k=1}^2 \delta_k^0 h^{(k)} = \begin{pmatrix} A_R & 0 & 0 \\ 0 & C_R & D_R \\ 0 & D_R & C_R \end{pmatrix} \quad (151)$$

5. Effective neutrino mass matrix

By direct computation, plugging Eqs. (145, 151) into the seesaw formula (Eq. 121) results in an effective neutrino mass matrix of the desired C1-pattern form:

$$M_\nu = \begin{pmatrix} M_{\nu 11} & M_{\nu 12} & M_{\nu 12}(1 + \chi) \\ M_{\nu 12} & M_{\nu 22} & M_{\nu 23} \\ M_{\nu 12}(1 + \chi) & M_{\nu 23} & M_{\nu 22} \end{pmatrix} \quad (152)$$

where the perturbation parameter χ is given by

$$\chi = \frac{\alpha(C_D - D_D)(C_R + D_R)}{(1 + \alpha)(C_R D_D - D_R C_D) + C_R C_D - D_R D_D} \quad (153)$$

Before ending this section, we would mention that introducing multiple Higgs doublets as we did in our constructions might display flavor-changing neutral currents. However, the effects are calculable in the models and in principle one can adjust the Yukawa couplings so that processes like $\mu \rightarrow e\gamma$ are suppressed [42]. Moreover, and as was discussed in the introduction, the RG running effects are expected to be small when multiple Higgs doublets are present, so that not to spoil the predictions of the symmetry at low scale.

10 Summary and Discussion

We have carried out a thorough phenomenological analysis for the patterns of the neutrino mass matrix meeting the $\mu - \tau$ symmetry. We found that exact symmetry leads to a totally degenerate spectrum and so is excluded on phenomenological grounds.

We thus introduced and in a minimal way perturbations such that the neutrino mass matrix satisfies an approximate $\mu - \tau$ symmetry. We got four such patterns and carried out a complete phenomenological analysis of them. We found that all these ‘deformed’ patterns can accommodate the current data without need to adjust the input parameters. However, no singular such patterns could meet the experimental constraints.

All the four patterns can produce all types of hierarchy and all have complex entries able to show CP-violation effects. The mixing angle θ_x can cover all its admissible range in all four patterns. As to the angle θ_y , it is unconstrained in the patterns C3 except that it should not equal the value 45° , whereas it is restricted to be around 45° , without taking this value, in the C1 pattern for the normal and inverted hierarchies, and around 36° or 52° in the C4 pattern of normal hierarchy type. Again, θ_y can not take the value 45° in the C2 pattern of normal or inverted hierarchy types, where it is just mildly constrained in the normal type to be around 45° . However, for this latter pattern C2, the mixing angle θ_z can not be larger than 10° . Actually, there is a narrow interval $]4^\circ, 4.7^\circ[$ for θ_z in the C4 pattern of normal type, whereas this mixing angle is bounded by 8° in the inverted type.

The phases are not constrained in the C3 or C4 patterns, except that in the C4 pattern of normal type the Dirac phase δ can not be in the interval $]160^\circ, 185^\circ[$ and the Majorana phase $\rho(\text{mod } \pi)$ can not belong to $] - 20^\circ, 20^\circ[$. As to the C1 pattern of normal type, the phases $\sigma, \rho(\text{mod } \pi)$ can not take values in the interval $] - 4^\circ, 4^\circ[$ around the origin, whereas the Dirac phase δ in all hierarchy types is

excluded from a narrow band $]177^0, 180.5^0[$ around π . For the C2 pattern, the phase ρ is excluded from the interval $]94^0, 99^0[$ in the degenerate case, and from broader intervals in the normal ($]90^0, 111^0[$) and inverted ($]48^0, 137^0[$) types. The phase $\sigma \pmod{\pi}$ is bound not to be around zero in the normal and inverted types, whereas the Dirac phase δ in all hierarchy types is excluded from narrow bands around zero ($] - 3^0, 1^0[$) and around π ($]178^0, 185^0[$).

There exist linear correlations between δ, ρ, σ for the patterns C1 and C3 in all types of hierarchy, and a linear correlation between $\langle m_{ee} \rangle$ and the **LNM** in the degenerate type for these two patterns.

The strength of the hierarchies is characterized by the ratio m_{23} , and the normal type hierarchy is usually mild taking values of order 1 in all patterns. However, the inverted hierarchy type in the patterns C1 and C3 can be very acute taking values of order $O(10^2)$.

All these features might help in distinguishing between the independent patterns. For example, if by measuring the mass ratios we find a very pronounced hierarchy, then we know that we have either C1 or C3 pattern, of an inverted hierarchy type. Consequently, if by measuring the angle θ_y we find a value far from 45^0 then we know we have a C3 pattern. Also if δ gives a value around π then again we have a C3 pattern. On the other hand, if by measuring the masses we get a mild hierarchy then we do not actually have enough signatures to determine the pattern. Rather, we have exclusion rules which help to drop as much patterns as possible. For example, if $\rho \pmod{\pi} \in] - 20^0, 20^0[$ or $\theta_z > 5^0$ or $\theta_y \neq 36^0, 52^0$ then we can drop the C4 pattern of normal type, whereas if $\theta_z > 8^0$ we exclude the C4 of inverted type possibility. If $|\rho \pmod{\pi}| < 4^0$ then no C1 pattern of normal type, while if $\rho \in]94^0, 99^0[$ then we drop the possibility of a C2 pattern. Also if $\theta_z \geq 10^0$ then we conclude that we do not have a C2 pattern of normal type. Moreover, the knowledge of all the phase angles and other mass parameters jointly and referring to the ‘narrow’ bands of the correlation plots can help in deciding which texture does fit the data.

We note finally that the deformation parameter $|\chi|$ can cover all its ‘perturbative’ range ($\leq 20\%$), except for the pattern C4 where it is bound to be a ‘tangible’ deformation ($|\chi| \geq 16\%$) in order to fit the experimental data.

All the perturbed patterns can be realized assuming exact $\mu - \tau$ symmetry augmented by new matter fields and abelian symmetries at the Lagrangian level, and we have presented some concrete examples using both types I and II of seesaw mechanism.

Our analysis follows a bottom-up approach and, in view of the full parameter space we adopted for the observables, can be considered as new. In particular, it shows in a very transparent way the correlation between the perturbation χ and the non-vanishing θ_z . We can summarize the mainly new results in our work as follows. First, we presented the complete analytical expressions (full or expanded) for all the observables and in all patterns. Second, we raised the question of convergence of the expansion series (Eq. 53) and analyzed it. Third, we presented an exhaustive analysis plotting all the possible correlations. Fourth, we disentangled the effects of the two perturbation parameters and presented detailed theoretical realizations of the resulting perturbed patterns. Fifth, we treated also the case of singular neutrino mass matrix. Sixth, we reached different conclusions compared to some other works with far more restricted parameter space.

Acknowledgements

Part of the work was done within the associate scheme and short visits program of ICTP. N.C. acknowledges funding provided by the Alexander von Humboldt Foundation.

References

- [1] Y. Fukuda *et al.*, Phys. Lett. B **436**, 33 (1998); Phys. Rev. Lett. **81**, 1562 (1998). For a review, see: C.K. Jung, C. McGrew, T. Kajita, and T. Mann, Ann. Rev. Nucl. Part. Sci. **51**, 451 (2001).
- [2] SNO Collaboration, Q.R. Ahmad *et al.*, Phys. Rev. Lett. **89**, 011301 (2002); Phys. Rev. Lett. **89**, 011302 (2002).
- [3] KamLAND Collaboration, K. Eguchi *et al.*, Phys. Rev. Lett. **90**, 021802 (2003).

- [4] K2K Collaboration, M.H. Ahn *et al.*, Phys. Rev. Lett. **90**, 041801 (2003).
- [5] CHOOZ Collaboration, M. Apollonio *et al.*, Phys. Lett. B **420**, 397 (1998); Palo Verde Collaboration, F. Boehm *et al.*, Phys. Rev. Lett. **84**, 3764 (2000).
- [6] T2K Collaboration, K. Abe *et al.*, Phys. Rev. Lett **107**, 041801 (2011).
- [7] MINOs Collaboration, P. Adamson *et al.*, Phys. Rev. Lett **107**, 181802 (2011).
- [8] DOUBLE-CHOOZ Collaboration, Y. Abe *et al.*, Phys. Rev. Lett **108**, 131801 (2012).
- [9] F. P. An *et al.*, [DAYA-BAY Collaboration], Phys. Rev. Lett **108**, 171803 (2012).
- [10] J. K. Ahn *et al.*, [RENO Collaboration], Phys. Rev. Lett. **108**, 191802 (2012).
- [11] See e.g., M. Hirsch, D. Meloni, S. Morisi, S. Pastor, E. Peinado, J. W. F. Valle, A. Adulpravitchai and D. Aristizabal Sierra *et al.*, arXiv:1201.5525 [hep-ph].
- [12] R. N. Mohapatra and S. Nussinov, Phys. Rev. D **60**, 013002 (1999); C. S. Lam, Phys. Lett. B **507**, 214 (2001); P. F. Harrison and W. G. Scott, Phys. Lett. B **547**, 219 (2002). T. Kitabayashi and M. Yasue, Phys. Rev. D **67**, 015006 (2003).
- [13] W. Grimus and L. Lavoura, JHEP **0107**, 045 (2001); W. Grimus and L. Lavoura, Phys. Lett. B **572**, 189 (2003); Y. Koide, Phys. Rev. D **69**, 093001 (2004); R. N. Mohapatra, JHEP **0410**, 027 (2004).
- [14] P. F. Harrison, D. H. Perkins and W. G. Scott, Phys. Lett. B **530**, 167 (2002).
- [15] V. D. Barger, S. Pakvasa, T. J. Weiler and K. Whisnant, Phys. Lett. B **437**, 107 (1998); A. J. Baltz, A. S. Goldhaber and M. Goldhaber, Phys. Rev. Lett. **81**, 5730 (1998).
- [16] C. H. Albright, A. Dueck and W. Rodejohann, Eur. Phys. J. C **70**, 1099 (2010).
- [17] Y. Kajiyama, M. Raidal and A. Strumia, Phys. Rev. D **76**, 117301 (2007); L. L. Everett and A. J. Stuart, Phys. Rev. D **79**, 085005 (2009).
- [18] E. Ma and M. Raidal, Phys. Rev. Lett. **87**, 011802 (2001); W. Grimus and L. Lavoura, JHEP **0107**, 045 (2001); E. Ma, Phys. Rev. D **66**, 117301 (2002); R. N. Mohapatra and S. Nasri, Phys. Rev. D **71**, 033001 (2005); R. N. Mohapatra, S. Nasri and H. -B. Yu, Phys. Lett. B **615**, 231 (2005); S. Nasri, Int. J. Mod. Phys. A **20**, 6258 (2005); T. Kitabayashi and M. Yasue, Phys. Lett. B **621**, 133 (2005); S. Choubey and W. Rodejohann, Eur. Phys. J. C **40**, 259 (2005); R. N. Mohapatra, S. Nasri and H. B. Yu, Phys. Lett. B **636**, 114 (2006); R. N. Mohapatra, S. Nasri and H. B. Yu, Phys. Lett. B **639**, 318 (2006); Z. -z. Xing, H. Zhang and S. Zhou, Phys. Lett. B **641**, 189 (2006); T. Ota and W. Rodejohann, Phys. Lett. B **639**, 322 (2006); Y. H. Ahn, S. K. Kang, C. S. Kim and J. Lee, Phys. Rev. D **73**, 093005 (2006); I. Aizawa and M. Yasue, Phys. Rev. D **73**, 015002 (2006); K. Fuki and M. Yasue, Phys. Rev. D **73**, 055014 (2006); K. Fuki and M. Yasue, R. Jora, S. Nasri and J. Schechter, Int. J. Mod. Phys. A **21**, 5875 (2006), Nucl. Phys. B **783**, 31 (2007); B. Adhikary, A. Ghosal and P. Roy, JHEP **0910** (2009) 040; Z. z. Xing and Y. L. Zhou, Phys. Lett. B **693**, 584 (2010); R. Jora, J. Schechter and M. Naeem Shahid, Phys. Rev. D **80**, 093007 (2009) [Erratum-ibid. D **82**, 079902 (2010)]; S. -F. Ge, H. -J. He and F. -R. Yin, JCAP **1005**, 017 (2010); I. de Medeiros Varzielas, R. González Felipe and H. Serodio, Phys. Rev. D **83**, 033007 (2011); H. -J. He and F. -R. Yin, Phys. Rev. D **84**, 033009 (2011); Y. H. Ahn, H. Y. Cheng, S. Oh, Phys. Lett. B **715**, 203 (2012); H. -J. He and X. -J. Xu, Phys. Rev. D **86**, 111301 (2012); S. Gupta, A. S. Joshipura and K. M. Patel, JHEP **1309**, 035 (2013); B. Adhikary, M. Chakraborty and A. Ghosal, JHEP **1310**, 043 (2013); C. Hamzaoui, S. Nasri and M. Toharia: arXiv:1311.2188 [hep-ph] (2013).
- [19] M. Abbas and A. Y. Smirnov, Phys. Rev. D **82** 013008 (2010)
- [20] E. I. Lashin, M. Abbas, N. Chamoun and S. Nasri, Phys. Rev. D **86** 033013 (2012), arXiv:1206.4754 [hep-ph].

- [21] E. I. Lashin, N. Chamoun and S. Nasri, Phys. Rev. D **86** 113013 (2012) , arXiv:1206.4754 [hep-ph].
- [22] J. Liao, D. Marfatia and K. Whisnant, Phys. Rev. D **87**, 013003 (2013).
- [23] S. Gupta, A. S. Joshipura, and K. M. Patel, JHEP **1309**, 035 (2013), arXiv:1301.7130 [hep-ph].
- [24] B. Adhikary, A. Ghosal and P. Roy, Int. J. Mod. Phys. **A 28** (2013) 24, 1350118
- [25] A. S. Joshipura, Eur. Phys. J. **C 53** (2008) 77,
- [26] R.N.Mohapatra and W. Rodejohann, Phys. Rev. D **72**, 053001 (2005) [hep-ph/0507312]; N. Haba and W. Rodejohann, Phys. Rev. D **74**, 017701 (2006) [hep-ph/0603206]; S. Luo and Z.-Z. Xing, Phys. Lett. B **646**, 242 (2007) [hep-ph/0611360]; Y. Koide and H. Nishiura, Int. J. Mod. Phys. A **25**, 3661 (2010) [arXiv:0911.2279].
- [27] W. Grimus and L. Lavoura, Eur. Phys. J. C **39**, 219 (2005) [hep-ph/0409231]
- [28] A. Dighe, S. Goswami and P. Roy, Phys. Rev. D **76**, 096005 (2007); S. Luo and Z. -z. Xing, Phys. Rev. D **86**, 073003 (2012).
- [29] W. Grimus and L. Lavoura, Fortsch. Phys. **61**, 535 (2013)
- [30] Z.Z. Xing; Phys. Lett. B **530** (2002), 159-166.
- [31] G. L. Fogli *et al.*, Phys. Rev. D **84**, 053007 (2011).
- [32] E. Lashin and N. Chamoun, Phys. Rev. D **85**, (2012) 113011.
- [33] C. Jarlskog, Phys. Rev. Lett. **55**, 1039 (1985); Z. Phys. C **29**, 491 (1985); Phys. Rev. D **35**, 1685 (1987).
- [34] G. L. Fogli, E. Lisi, A. Marrone, D. Montanino, A. Palazzo and A. M. Rotunno, Phys. Rev. D **86**, 013012 (2012).
- [35] T. Schwetz, M. Tortola and J. W. F. Valle, New J. Phys. **13**, 063004 (2011); T. Schwetz, M. Tortola and J. W. F. Valle, New J. Phys. **13**, 109401 (2011); D. V. Forero, M. Tortola and J. W. F. Valle, Phys. Rev. D **86**, 073012 (2012).
- [36] M. C. Gonzalez-Garcia, M. Maltoni and J. Salvado, JHEP **1004**, 056 (2010); M. C. Gonzalez-Garcia, M. Maltoni, J. Salvado and T. Schwetz, JHEP **1212**, 123 (2012).
- [37] G. L. Fogli *et al.*, Phys. Rev. D **78**, 033010 (2008).
- [38] E. Andreotti *et al.*, Astropart. Phys. **34**, 822 (2011).
- [39] Z.Z. Xing; Phys. Rev. D **78**, 011301(R) (2008).
- [40] T. P. Cheng and L. F. Li, Phys. Rev. D **22**, 2860 (1980); R. N. Mohapatra and G. Senjanovic, Phys. Rev. D **23**, 165 (1981).
- [41] E. I. Lashin, N. Chamoun, E. Malkawi and S. Nasri, Phys. Rev. D **83**, 013002 (2011)
- [42] C. Hagedorn, J. Kersten and M. Lindner, Phys. Lett. B **597**, 63 (2004)